

## RESEARCH ARTICLE

10.1002/2017JA024147

## Key Points:

- First observation of energy-banded ions at Saturn
- Banded ions are  $H^+$  but cannot tell if other species are similarly banded
- Band energies are consistent with a bounce-resonant interaction with the standing wave of a field line resonance

## Correspondence to:

M. F. Thomsen,  
mthomsen@psi.edu

## Citation:

Thomsen, M. F., S. V. Badman, C. M. Jackman, X. Jia, M. G. Kivelson, and W. S. Kurth (2017), Energy-banded ions in Saturn's magnetosphere, *J. Geophys. Res. Space Physics*, 122, 5181–5202, doi:10.1002/2017JA024147.







Received 14 MAR 2017

Accepted 24 APR 2017

Accepted article online 27 APR 2017

Published online 11 MAY 2017

## Energy-banded ions in Saturn's magnetosphere

M. F. Thomsen<sup>1</sup> , S. V. Badman<sup>2</sup> , C. M. Jackman<sup>3</sup> , X. Jia<sup>4</sup> , M. G. Kivelson<sup>4,5</sup> , and W. S. Kurth<sup>6</sup> 
<sup>1</sup>Planetary Science Institute, Tucson, Arizona, USA, <sup>2</sup>Department of Physics, University of Lancaster, Lancaster, UK,

<sup>3</sup>Department of Physics and Astronomy, University of Southampton, Southampton, UK, <sup>4</sup>Climate and Space Sciences and Engineering, University of Michigan, Ann Arbor, Michigan, USA, <sup>5</sup>Earth Planetary and Space Sciences, University of California, Los Angeles, California, USA, <sup>6</sup>Department of Physics and Astronomy, University of Iowa, Iowa City, Iowa, USA

**Abstract** Using data from the Cassini Plasma Spectrometer ion mass spectrometer, we report the first observation of energy-banded ions at Saturn. Observed near midnight at relatively high magnetic latitudes, the banded ions are dominantly  $H^+$ , and they occupy the range of energies typically associated with the thermal pickup distribution in the inner magnetosphere ( $L < 10$ ), but their energies decline monotonically with increasing radial distance (or time or decreasing latitude). Their pitch angle distribution suggests a source at low (or slightly southern) latitudes. The band energies, including their pitch angle dependence, are consistent with a bounce-resonant interaction between thermal  $H^+$  ions and the standing wave structure of a field line resonance. There is additional evidence in the pitch angle dependence of the band energies that the particles in each band may have a common time of flight from their most recent interaction with the wave, which may have been at slightly southern latitudes. Thus, while the particles are basically bounce resonant, their energization may be dominated by their most recent encounter with the standing wave.

**Plain Language Summary** During an outbound passage by the Cassini spacecraft through Saturn's inner magnetosphere, ion energy distributions were observed that featured discrete flux peaks at regularly spaced energies. The peaks persisted over several hours and several Saturn radii of distance away from the planet. We show that these "bands" of ions are plausibly the result of an interaction between the Saturnian plasma and standing waves that form along the magnetospheric magnetic field lines. These observations are the first reported evidence that such standing waves may be present in the inner magnetosphere, where they could contribute to the radial transport of Saturn's radiation belt particles.

## 1. Introduction

The inner magnetosphere of Saturn is characterized by several different plasma populations [e.g., Young *et al.*, 2005], including a dense, cool component that is locally produced by ionization of neutral water vapor vented by Saturn's moon Enceladus [e.g., Porco *et al.*, 2006; Waite *et al.*, 2006; Sittler *et al.*, 2008], and a suprathermal, more tenuous component that is primarily injected from the outer magnetosphere in discrete, centrifugally driven interchange events [e.g., Burch *et al.*, 2005; Hill *et al.*, 2005]. The cool ion population is dominantly composed of water group ions ( $O^+$ ,  $OH^+$ ,  $H_2O^+$ , and  $H_3O^+$ , commonly denoted " $W^+$ ") and  $H^+$ , with a lesser contribution of  $H_2^+$  [e.g., Sittler *et al.*, 2005; Thomsen *et al.*, 2010], plus other minor ions such as  $N^+$  and  $O_2^+$ .

Saturn's strong magnetic field, combined with good ionospheric conductivity, couples the rapid planetary rotation to the magnetospheric plasma, which is observed to flow with nearly the rigid corotational azimuthal velocity in the inner magnetosphere ( $\lesssim 10$ ) [e.g., Sittler *et al.*, 2005; Wilson *et al.*, 2008, 2009; Thomsen *et al.*, 2010; Livi *et al.*, 2014]. Ionization of neutrals in this environment results in new "pickup" ions, which occupy a ring in velocity space that convects with the near-corotational bulk flow speed and has a ring speed equal to that bulk flow speed [e.g., Tokar *et al.*, 2008]. Such distributions thermalize rather quickly, resulting in a population with a thermal speed comparable to the bulk flow speed, still convecting with the flow. The average energy per particle of a pickup ion population should thus be approximately twice  $0.5m_iV_c^2$ , where  $m_i$  is the mass of the ion and  $V_c$  is the bulk flow speed of the plasma. Voyager and typical Cassini observations [e.g., Bridge *et al.*, 1981; Young *et al.*, 2005] do indeed show two peaks in energy-per-charge space, located just above the corotational energy for  $H^+$  and  $W^+$ , and rising with increasing radial distance as  $V_c$  itself rises (since  $V_c \sim r\Omega_S$ , where  $\Omega_S$  is Saturn's angular velocity).

While the relative fractions of thermal  $W^+$  and  $H^+$  vary with latitude because the heavy ions tend to be centrifugally confined more closely toward the equatorial plane than are the light ions [e.g., *Thomsen et al.*, 2010], the two-peaked structure of the ion  $E/q$  spectrum (with the energy of the peaks increasing with radial distance) is seen during almost every Cassini pass through the inner magnetosphere. In this paper we report observations from one of the rare exceptions to this rule: On 3 May 2005, as Cassini was outbound through the near-midnight sector at a magnetic latitude  $\sim 20^\circ$ , the cool ion distribution was observed to consist of  $\sim 3$ – $4$  discrete bands in  $E/q$ . The band energies uniformly decreased with increasing radial distance, but they appeared superimposed on a background thermal population that followed the expected general increase with  $r$ . The bands persisted over at least 4 h, as Cassini covered the radial range from  $L \sim 5.6$  to  $7.5$  (where  $L$  is the equatorial crossing point in Saturn radii,  $R_S$ , of a dipole field line through Cassini's position) and the latitude range from  $\sim 21.8^\circ$  to  $18.1^\circ$ .

Energy-banded ions have been seen under a number of different circumstances in the Earth's magnetosphere [see *Colpitts et al.*, 2016, for a review]. They have been reported during both quiet and geomagnetically active intervals; in the auroral zone, at subauroral latitudes, and near the dayside magnetopause, and at ion energies of tens of eV to tens of keV. In some cases composition measurements show that  $O^+$  and  $H^+$  bands have the same energy, while other occurrences show  $O^+$  and  $H^+$  having the same velocities. Still other studies show that  $O^+$  and  $H^+$  have different occurrence probabilities and locations. In some observations the ions are peaked at  $90^\circ$  pitch angles, whereas in others they appear dominantly field aligned. Events can be very long lasting, up to 12 h, and often are extensive in both latitude and magnetic local time.

A number of possible generation mechanisms for energy-banded ions at Earth have been proposed (also reviewed by *Colpitts et al.* [2016]), including convective drift dispersion or time-of-flight dispersion from either an ionospheric or an equatorial heating event. The different generation scenarios have different implications for the properties of the banded ions, and some observational support seems to exist for essentially all of the mechanisms.

While energy-banded ions of various properties are well documented in the Earth's magnetosphere, no such phenomena have yet been reported in the giant magnetospheres of Jupiter and Saturn. The purpose of the present paper is to report the observation by Cassini of such an event in Saturn's inner magnetosphere and to examine the properties of the banded ions.

## 2. Observations

The observations presented in this study come primarily from the Cassini Plasma Spectrometer (CAPS) instrument on the Cassini spacecraft, which has been in orbit around Saturn since mid-2004. CAPS consists of three separate sensors: the ion beam spectrometer, the electron spectrometer, and the ion mass spectrometer (IMS) (see *Young et al.* [2004] for details on the instrumentation). In this report we focus on data from the IMS, which is a top-hat electrostatic analyzer to measure the energy per charge of incident ions, followed by a time-of-flight (TOF) section to determine their speed and hence their mass per charge. The instantaneous field of view (FOV) of the IMS is segmented into eight separate angular channels viewing different directions in velocity space. Under normal operating conditions, a physical actuator on CAPS sweeps the FOV across the sky, resulting in solid-angle coverage of  $\sim 2\pi$  sr for the full actuation cycle.

The IMS produces several different data products with different cadences that are determined by the telemetry rate. "Singles" (SNG) data are obtained from the start signals in the TOF section, so they yield only the energy per charge of the ions and not their mass. They do, however, provide information about the angular distribution of the particles. SNG data cover 64 contiguous, logarithmically spaced energy channels between  $\sim 1$  eV and  $\sim 50$  keV for each of the eight IMS anodes, summed over an actuation-angle range that depends on the telemetry.

The TOF data provide mass determination, but because of the lower efficiency for this measurement, the TOF data product is summed on board over all look directions (all 8 detectors and all actuation angles) for either 512 s or 256 s, depending on the telemetry. The ion distribution is further summed in energy, reducing the native 64 channels to 32. A TOF data product therefore consists of counts in a matrix of 32  $E/q$  levels by 256 time-of-flight channels, enabling identification of the  $m/q$  of the various particles but no information about their angular distribution.

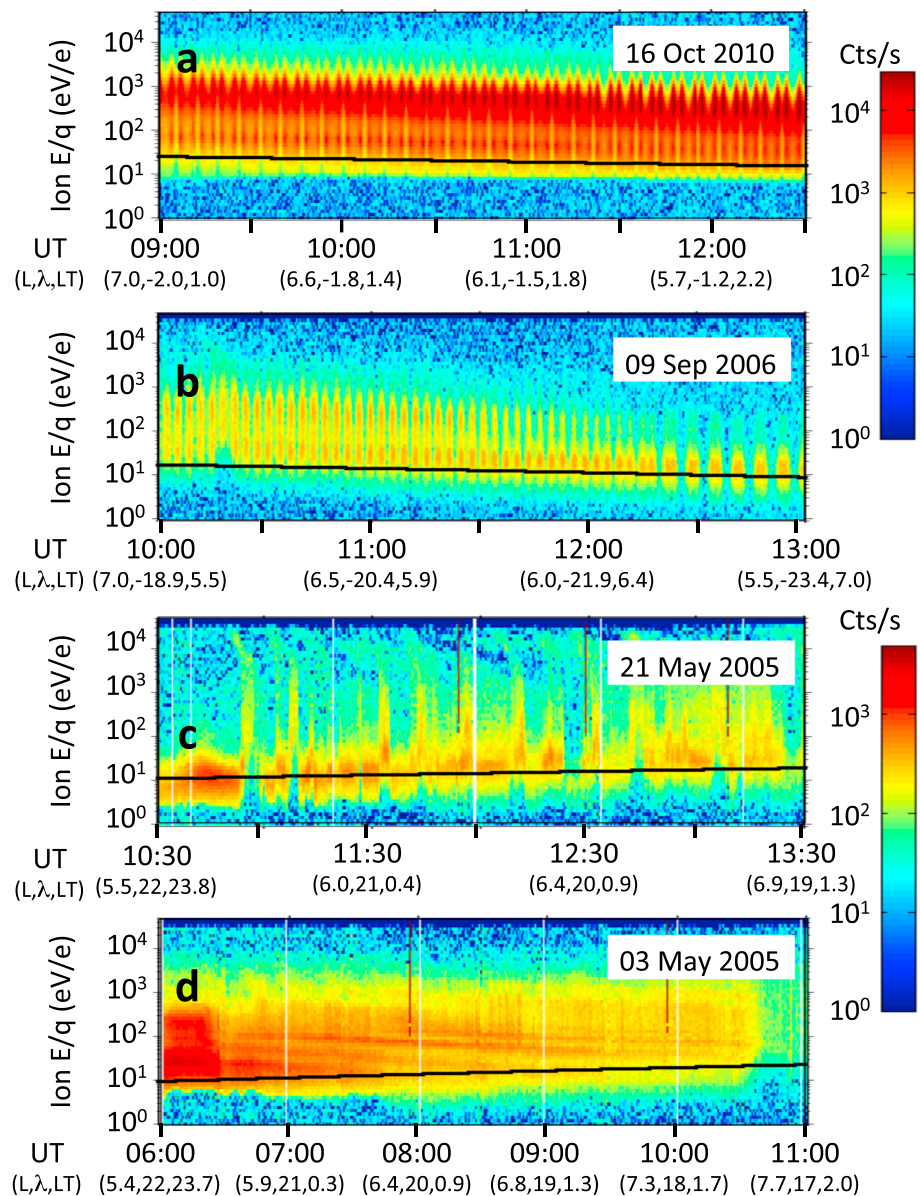


**Figure 1.** Color-coded count rate (proportional to energy flux) for ions observed by the Cassini/CAPS IMS on several passes through the inner magnetosphere: (a) 16 October 2010, (b) 9 September 2006, (c) 21 May 2005, and (d) 3 May 2005. Periodic structure seen in Figures 1a and 1b is due to the actuation of the instrument, allowing the detectors to view different directions in space. CAPS was not actuating during the two intervals in Figures 1c and 1d. The solid black line in each panel gives the local corotational energy of a proton. Figure 1d shows a set of discrete energy bands, with band energies that decrease with increasing radial distance. The spacecraft location in  $L$ , magnetic latitude ( $\lambda$ ), and local time is indicated below the time axis.

Whenever a TOF data product is reported, CAPS also reports an ION data product, which involves an onboard sorting of the counts into  $m/q$  bins based on the measured  $E/q$  and TOF, much as is done on the ground with the TOF data product [e.g., *Thomsen et al.*, 2014]. The ION data product is similar to the SNG product in that the energy spectrum is reported for each of the eight anodes, providing information on the angular distribution of each species, but the count rates are typically quite low unless the fluxes are very high. We are able to make only limited use of this capability in the present study.

In addition to the CAPS data, we will present corresponding observations from the Cassini magnetometer (MAG) [*Dougherty et al.*, 2004] and the Radio and Plasma Wave Investigation (RPWS) [*Gurnett et al.*, 2004].

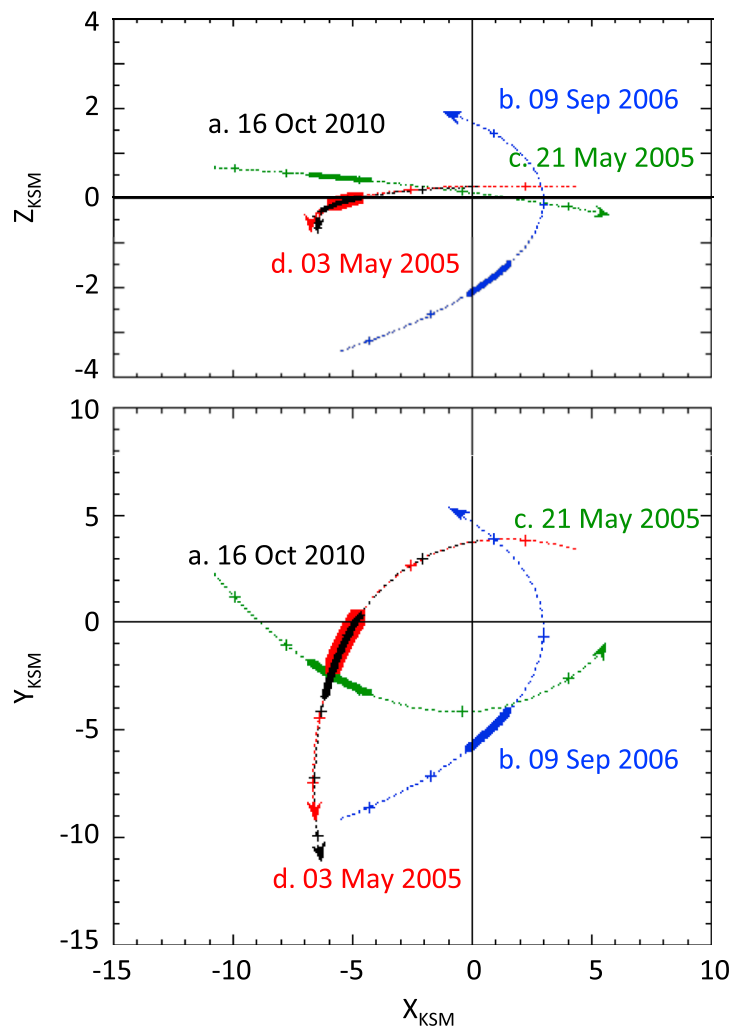


**Figure 2.** KSM (Kronocentric solar magnetospheric) X-Z and X-Y projections of Cassini orbits for the days shown in Figure 1. Each trajectory segment covers a full day (00–24 h). Heavy portions of each curve correspond to the actual time ranges from Figure 1. The sun is to the right of the figure. Plus markers on each curve do not indicate specific times (e.g., hours of the day) but are simply present to help identify the curves.

Figure 1a shows IMS observations for a typical low-latitude, nightside pass through Saturn's inner magnetosphere. The panel shows the color-coded SNG count rate from IMS anode 1 for 3.5 h during an inbound pass on 16 October 2010. Between 0900 and 1300 UT, Cassini moved from  $L \sim 7.00$  to  $L \sim 5.25$ , at a magnetic latitude  $\sim -1^\circ$  to  $-2^\circ$  and a local time of  $\sim 01$ – $03$  LT (cf. Figure 2, black curve). The count rate is shown as a function of the ion  $E/q$  on the vertical axis and time on the horizontal axis. The solid black line superimposed on the spectrogram shows the local corotational energy of a proton ( $0.5m_p\rho^2\Omega_S^2$ ), where  $\rho = r\cos\lambda$ , with  $\lambda$  the latitude of the spacecraft and  $r$  its radial distance from Saturn. The  $W^+$  corotational energy would be a factor of  $\sim 16$  above the  $H^+$  value shown in the figure. The ion spectra in Figure 1a exhibit a double-peaked character in  $E/q$ . As described above, the two peaks correspond to  $H^+$  (below  $\sim 100$  eV/e) and  $W^+$  (above  $\sim 100$  eV/e). As expected for thermalized pickup ion distributions observed with an electrostatic analyzer, the peak count rates (proportional to the energy flux) are found near 4 times the corotational energy of each species, decreasing as the spacecraft approaches Saturn. The periodic variations in the count rate are produced as the actuator scans the FOV of the instrument through different look directions.

During the interval in Figure 1a, CAPS was able to view the corotational direction of motion, so the bulk of the transsonic distribution lies within the FOV, accounting for the high count rates. At these low latitudes,  $W^+$  dominates the  $E/q$  spectra because it is more confined to the magnetic equator by centrifugal force than is

the  $H^+$  (e.g., see the species-dependent scale heights derived by *Thomsen et al.* [2010]). But the two-peak character of the  $E/q$  distribution is quite clear.

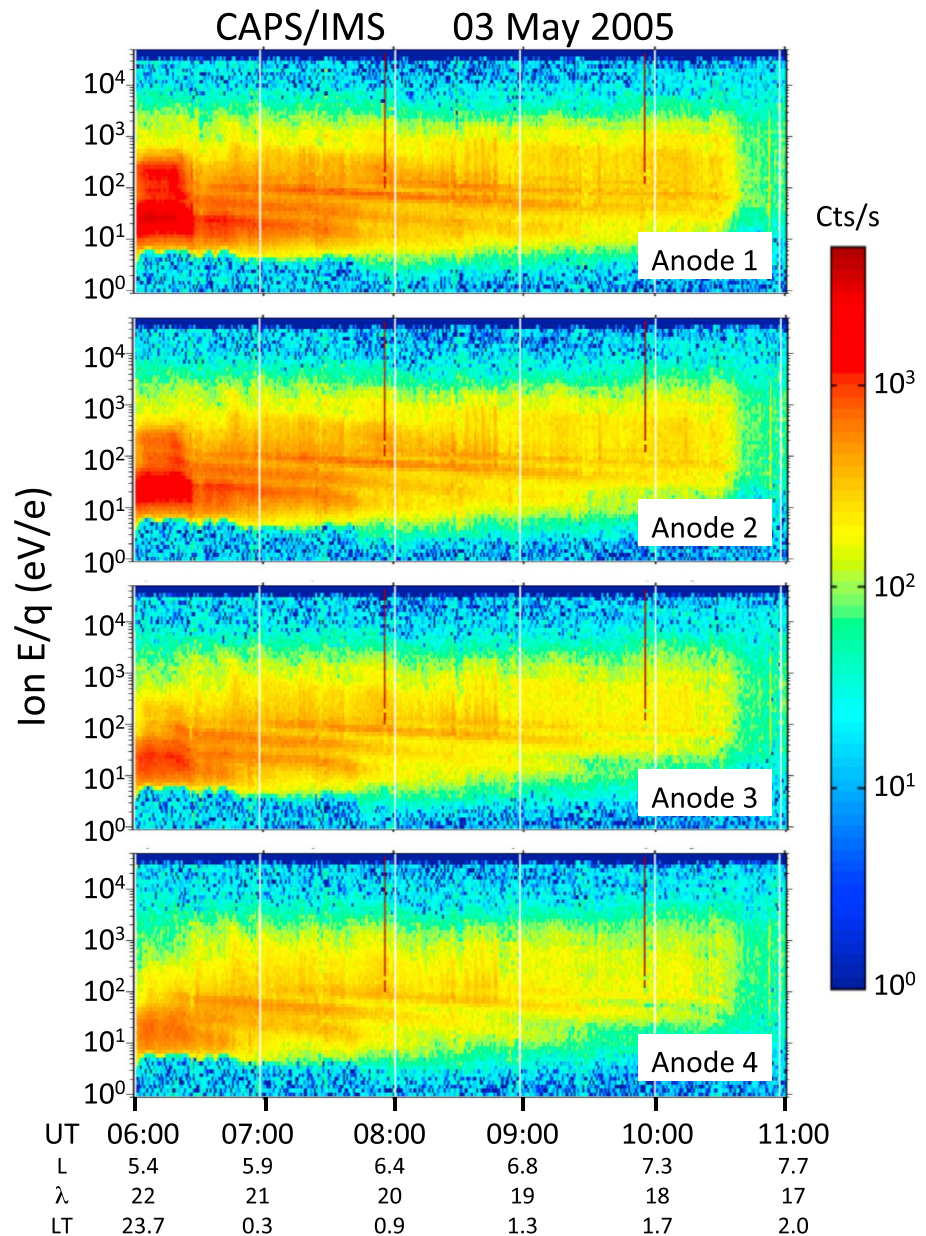
Figure 1b shows a similar spectrogram for a typical higher-latitude inbound pass near dawn on 9 September 2006, in this case from anode 7. During the interval shown, the spacecraft moved from ( $L, \lambda, LT$ ) of (7.0,  $-18.9^\circ$ , 5.5) to (5.5,  $-23.4^\circ$ , 7.0) (see Figure 2, blue curve). Again the viewing was favorable for seeing the corotating transsonic distribution, with periodic variations due to the actuation of the instrument. Due to the higher latitude,  $W^+$  is no longer the dominant ion in the spectrogram, with the  $H^+$  peak (lower energies) as intense or even more intense than the  $W^+$  (upper energies). As in Figure 1a, it is clear that the ion populations peak at  $E/q$  near and above their corresponding corotational energies, decreasing with declining distance from the planet. (The spectral event near 1020 UT is an example of the centrifugally driven interchange injection events mentioned in the introduction and is not relevant to the present discussion.)

Figure 1c shows a third spectrogram, from anode 1 for an outbound pass on 21 May 2005, during which Cassini moved from ( $L, \lambda, LT$ ) of (5.5,  $22^\circ$ , 23.8) to (6.9,  $19^\circ$ , 1.3) (see Figure 2, green curve). For this interval, CAPS was not actuating and did not view directly into the corotational direction. There are numerous interchange injections, but the cool plasma is still visible between events. There is little cool  $W^+$  observed due to the high latitude and poor viewing, but the energy of the cool  $H^+$  tracks the corotational energy quite well, increasing with increasing radial distance, as was the case for the other intervals shown in Figures 1a and 1b (in this case, since the instrument was looking essentially perpendicular to the flow, the peak count rate is seen at less than 4 times the corotational energy, as one would expect).

Finally, Figure 1d shows a spectrogram from anode 1 obtained on 3 May 2005, during which Cassini was outbound through the same general  $L$  range as the other panels in Figure 1, moving from ( $L, \lambda, LT$ ) of (5.4,  $22^\circ$ , 23.7) to (7.7,  $17^\circ$ , 2.0) (see Figure 2, red curve). On this pass, which immediately preceded the pass shown in Figure 1c and had very similar orbital parameters, the ion  $E/q$  distribution looks quite different from that seen on the previous orbit. CAPS was again not actuating, but prior to 0630 UT, anode 1 was looking only slightly off the corotation direction, and strong fluxes were seen in both the  $H^+$  and  $W^+$  populations, with  $H^+$  dominating at this high latitude. During this interval, the  $E/q$  distribution showed two peaks, corresponding to corotating pickup  $H^+$  and  $W^+$ , as in the other panels. After 0630 UT, the spacecraft executed a roll such that neither anode 1 nor any of the other anodes was viewing near the corotation direction, and the fluxes dropped accordingly. Further, with the anodes now looking well away from corotation, a different energy structure appears in the distribution: There are now three distinct bands of ions, with energies that decrease with increasing radial distance instead of increasing in correspondence with the corotational energy. Moreover, at  $\sim 0800$  UT the bottom energy band disappears and is replaced by an additional band above 100 eV. This disappearance of the lowest-energy band and replacement with a new highest-energy band was repeated at least once more before  $\sim 1040$  UT, when another spacecraft roll moved the IMS FOV into the direction opposite corotation, and the fluxes became quite low. All of these bands occupy the same general range of energies occupied by the thermal plasma at lower latitudes (cf. Figures 1a and 1b), but the band energies clearly decrease with time and increasing radial distance. The bands seem to disappear when the band energy falls below the local corotational energy (black line). The peak-to-trough flux amplitudes of the bands are a few percent to about 20%.

Figure 3 focuses on this interval from 3 May 2005 in more detail, with views from four different anodes presented in separate panels. As shown there, the level of the fluxes decreased for progressively higher anode numbers, which correspond to view directions closer to the magnetic field. Anodes 5–8 likewise saw the bands, but at even lower fluxes. A detailed examination of the count rate  $E/q$  spectra (not shown) reveals that the peaks are not seen at exactly the same energy in the various anodes; rather, there is a slight but systematic and progressive shift in energy from anode 1 to the other anodes. We will return to this point below when we discuss the pitch angle distribution of the banded ions, but we bring it up here because it has implications for analysis of the composition of the bands, to which we turn next.

As described above and in greater detail by *Thomsen et al.* [2014], the TOF data product enables determination of the composition of the ions measured by CAPS, albeit with no angular information and with reduced energy resolution. Figure 4 shows the energy distribution of the counts in the three main ion species ( $H^+$ ,  $H_2^+$ , and  $W^+$ ) for a representative interval during the banded ion event, computed following the procedure



**Figure 3.** Color-coded count rate spectrograms from four different CAPS/IMS anodes with different look directions for the 3 May 2005 interval shown in Figure 1d.

described in *Thomsen et al.* [2014]. The two vertical bars span the range of energies of the highest-energy clear peak in the SNG spectrum for all the anodes over this time range. The other clear peaks were all at lower energies than these bars, and it is clear from the figure that in the range of energies where the bands are observed  $H^+$  is by far the dominant contributor to the counts. There is a small peak between the vertical bars in Figure 4, but the band structure is far from obvious, first because the TOF product sums over two adjacent energy channels, so the energy resolution is intrinsically lower than for SNG data, and second because the TOF product sums over all the anodes, which as noted above see the band peaks at slightly different energies, further smearing the structure in energy. Nonetheless, from Figure 4 it is clear that the bands that are seen in SNG are primarily in the  $H^+$  population. There may also be bands in the other species, but the energy resolution of the TOF data product is not adequate to say definitively whether or not this is the case. Examination of the ION data product mentioned above (not shown) confirms that the onboard-sorted  $H^+$  does in fact display the same peaks as the SNG spectra, but with

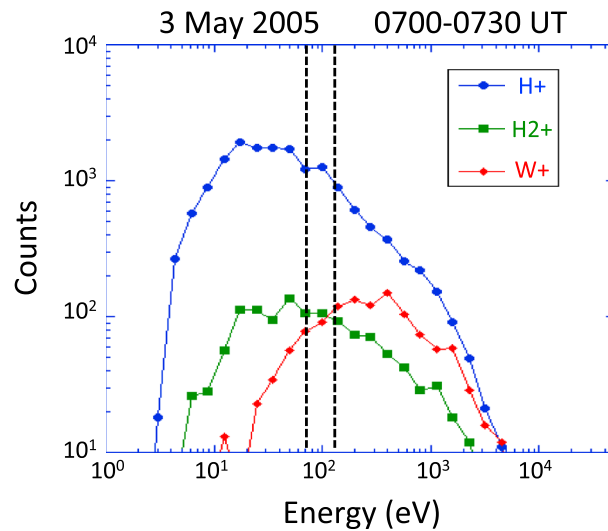


**Figure 4.** Thirty minute sum of counts in the TOF data product, sorted into species bins according to the procedure described in *Thomsen et al.* [2014]. Vertical bars span the range of energies of the first clear banded-ion peak in the SNG spectrum for all the anodes over this time range.

much lower count rates. The count rates in the ION  $W^+$  and  $H_2^+$  spectra are too low to draw meaningful conclusions about whether or not bands exist in those species.

Returning to the energies of the bands, it is important to realize that these are the particle energies as seen in the frame of the spacecraft. Since the plasma is approximately corotating with Saturn, it is necessary to transform into the corotating frame to examine the true band energies and pitch angles. Ideally, one would transform into the plasma rest frame, but because the actuator was not operating during this interval, we are unable to obtain bulk flow moments of the distribution [e.g., *Thomsen et al.*, 2010] and have simply assumed full corotation to do the transformation. While several studies have

shown that the flow speed in this region of the magnetosphere is actually more typically  $\sim 60\text{--}90\%$  of full corotation [e.g., *Wilson et al.*, 2008, 2009; *Thomsen et al.*, 2010; *Holmberg et al.*, 2012], the assumption of full corotation as opposed to 60% makes only a small quantitative difference (few degrees in pitch angle and few percent in energy). The SNG measurements have accordingly been transformed to the corotating frame, and the energies of the peaks in that frame have been tabulated at 15 min intervals during the 3 h period from 0630 to 0930 UT.

Figure 5 summarizes the resulting band energies in the corotating frame. Figure 5a shows the band energies for the four anodes with the highest counting rates, plotted as a function of time during the 3 h interval. Even in the corotating frame, it is clear that the band energies vary with look direction. The solid line in Figure 5a is the  $H^+$  corotation energy over the same time range, showing the increase with time that contrasts clearly with the decrease seen in the band energies. Figure 5b shows the band energies as a function of time for just anode 1, which has the highest count rates. The bands show a very clear and near-exponential decrease with time during the interval. Because of the nature of Cassini's orbit at this time, both the  $L$  value and the latitude of the spacecraft varied monotonically with time, and Figures 5c and 5d show the anode 1 band energies plotted as a function of  $L$  and latitude, respectively. These also yield nearly exponential dependences of the band energies, decreasing with  $L$  and increasing with latitude. The coupling of these parameters makes it impossible to determine which dependence is primary ( $t$ ,  $L$ , or  $\lambda$ ). Table 1 provides the coefficients of exponential fits to the three parameters for the three anode-1 bands highlighted in Figures 5b–5d. Based on these fits for anode 1, the average ratio of the band 2 (middle) energy to the band 1 (lowest) energy is  $\sim 2.0$ , and the average band 3 (highest) to band 2 ratio is  $\sim 2.5$ .

In addition to calculating the band energies in the corotating frame, we have also calculated the pitch angles seen by each of the anodes in this frame. We have then binned the observed counts into energy and pitch angle bins for 5 min intervals during the pass. Figures 6a–6c show the count rate as a function of energy and pitch angle bin for three different 5 min intervals during the time when the ion bands were seen. The bands can be seen in each panel; moreover, all three panels show that the energy of the bands appears to decrease with increasing pitch angle, even across  $90^\circ$ . This is confirmed by Figures 6d–6f, which show the band energies vs pitch angle for three of the individual spectra summarized in Figure 5a. In Figures 6d–6f, we have connected points corresponding to the same apparent band in order to guide the eye, but the bands clearly follow the same behavior seen in the 5 min summed pitch angle plots in Figures 6a–6c. Note that for Cassini's location at northern latitudes at this time, particles with pitch angles less than  $90^\circ$  are moving toward the equator, whereas those with pitch angles greater than  $90^\circ$  are moving away from the equator.

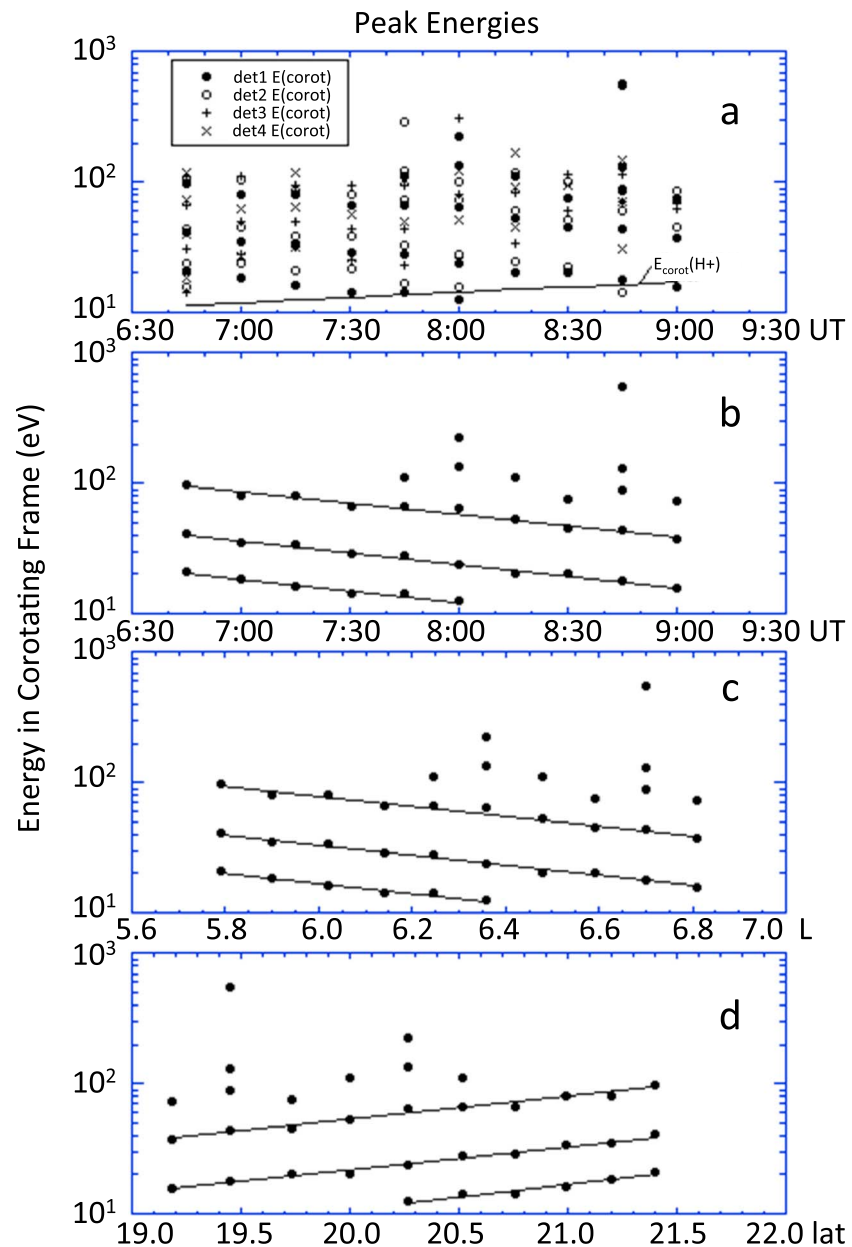


**Figure 5.** (a) Energy of the peak count rate in each of the ion bands seen in the four anodes shown in Figure 3, plotted versus time on 3 May 2005; (b) same as Figure 5a for only anode 1; (c) same band energies from anode 1 plotted as a function of  $L$ , which increased monotonically with time during the interval; (d) same band energies from anode 1 plotted as a function of magnetic latitude, which decreased monotonically during the interval. All band energies have been computed in the corotating frame of reference. The line in Figure 5a is the  $H^+$  corotation energy over the same time range. Lines in the other three panels are drawn to guide the eye in recognizing the discrete energy bands. Table 1 provides the coefficients of exponential fits to the three highlighted bands.

Further, Figures 6a–6c show that the energy flux (proportional to the color-coded counts) is greater for particles coming from the equator (pitch angle  $> 90^\circ$ ) than for those coming from high latitudes (pitch angle  $< 90^\circ$ ) at the same  $|\text{pitch angle} - 90^\circ|$ .

### 3. Discussion

#### 3.1. Other Events

We have not conducted a comprehensive survey for additional such banded-ion events, but Table 2 lists the few intervals where we have seen banding while surveying the data for other purposes. None of these

**Table 1.** Exponential Fits to Anode 1 Band Energies:  $E = a \exp(-bx)$ 

	Band 1	Band 2	Band 3
$x = t$			
$a(\text{eV})$	316	631	1438
$b(\text{s}^{-1})$	$-1.13 \times 10^{-4}$	$-1.13 \times 10^{-4}$	$-1.11 \times 10^{-4}$
$R$	0.980	0.991	0.982
$x = L$			
$a(\text{eV})$	3426	7212	15755
$b(R_S^{-1})$	-0.885	-0.896	-0.881
$R$	0.981	0.991	0.982
$x = \lambda$			
$a(\text{eV})$	$1.60 \times 10^{-3}$	$6.20 \times 10^{-3}$	$1.67 \times 10^{-2}$
$b(\text{degree}^{-1})$	0.441	0.409	0.403
$R$	0.970	0.990	0.982

additional intervals shows the bands quite as clearly as the 3 May 2005 event described above, nor have we done such a complete analysis of the band properties in those events. For the remainder of this paper, we focus on the 3 May 2005 event, but the other events may yield additional relevant information in the future.

### 3.2. Transport of Banded Ions

In addition to the observational features described above regarding the banded ions, consideration of the band energies (in the corotating frame) provides additional insight. We focus first on locally mirroring particles (i.e., with pitch angles of  $90^\circ$ ). We obtain the band energies for those particles by interpolating along energy-versus-pitch angle curves such as those shown in Figures 6d–6f. Using a dipole approximation for the magnetic field, which is valid within the radial range of interest [Burton *et al.*, 2010], we estimate the equatorial pitch angle corresponding to locally mirroring particles. Combining the equatorial pitch angle and the inferred band energy for locally mirroring particles, we estimate the travel time from the equator to the observation point for  $\text{H}^+$  ions at each of the 15 min intervals shown in Figure 5. For locally mirroring particles this is

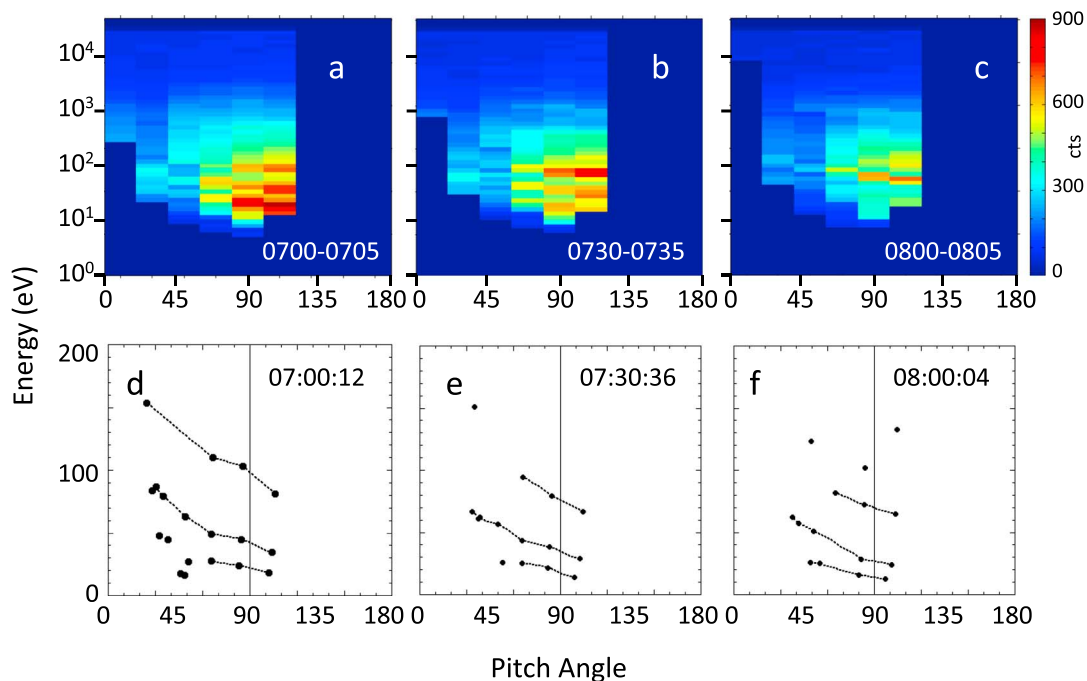


**Figure 6.** Five minute accumulations of color-coded counts from SNG data, sorted into energy and pitch angle bins in the corotating frame: (a) 0700–0705 UT, (b) 0730–0735 UT, and (c) 0800–0805 UT. (d–f) The energy in the corotating frame of the identified bands at times corresponding to Figures 6a–6c, respectively, plotted as a function of pitch angle in the corotating frame. For the spacecraft located at northern latitudes, pitch angles less than  $90^\circ$  correspond to particle moving southward toward the equator, whereas pitch angles greater than  $90^\circ$  correspond to particles moving northward away from the equator. Particles moving away from the equator show larger count rates and lower band energies than those moving toward it.

**Table 2.** Other Candidate Banded-Ion Events

Date	Time Range	Latitude	Local Time	<i>L</i> Range	Notes
25 Jul 2006	0800–1110	11°	18	7.8–9.4	Weak
9 Nov 2006	0630–0800	26°	16	7.1–8.8	
3 Dec 2006	0430–0700	28°	15	7.5–11	
24 Nov 2008	0400–0540	29°	22	6.6–9.1	High telemetry rate

just one-fourth bounce period, where the latter is calculated according to *Thomsen and Van Allen* [1980]. The results are shown in Figure 7a for four identifiable bands, with band 1 being the lowest-energy one.

Subtracting this direct travel time from the time of observation, we find the most recent time at which particles in each band would have left the equator on their way to the spacecraft. These equatorial departure times (in seconds of the day) are shown in Figure 7b. This calculation reveals that the slowest particles seen by Cassini at 0645 UT (band 1) left the equator at ~0530 UT, while particles in the most energetic band seen at 0645 (band 3) left the equator at ~0608 UT. Assuming full corotation (and ignoring gradient and curvature drifts, which are negligible in this energy range), the direct travel times combined with the local time of observation also determine the local time at which the banded ions left the equatorial plane. These are shown in Figure 7c. Note that although the energy-banded ions were observed by Cassini near local midnight, the travel time from the equator is so long for these energies that the original departure from the equator actually occurred near LT ~ 21 for the lowest-energy band.

Finally, Figure 7d shows the difference in the equatorial departure time between pairs of adjacent bands. At least for the lowest three bands (1–3), the inferred departure times are separated by ~1200–1700 s, apparently increasing with time or radial distance.

The solid line shown in Figure 7d is the travel time for an Alfvén wave to propagate along the field line from the equator to a high-latitude mirror point and back to the equator. To find this time, we combined the radial dependence of the equatorial densities of the three main ion species determined by *Thomsen et al.* [2010] and shown in their Figure 7c with the scale heights also given in that figure to calculate the plasma mass density as a function of latitude along a given dipole magnetic field line in the inner magnetosphere. The corresponding Alfvén speed as a function of *L* and  $\lambda$  was then calculated, and the travel time was integrated over one half the bounce period, yielding the curve shown in Figure 7d.

### 3.3. Possible Scenario: Field Line Resonance

The half-bounce Alfvén time in Figure 7d is of the same order as the time difference between successive equatorial departure times for the banded ions, and it has the same radial dependence. This suggests that the bands may be produced by acceleration/deceleration within a large-scale field line resonance (FLR). FLRs are standing shear Alfvén waves with parallel wave numbers that are quantized by the ionospheric boundary conditions [e.g., *Chen and Hasegawa*, 1974; *Southwood*, 1974; *Kivelson and Southwood*, 1985; *Hughes*, 1994]. The fundamental mode ( $n = 1$ ) has one half wavelength between ionospheric boundaries, and the second harmonic ( $n = 2$ ) has a full wavelength between ionospheric boundaries. The corresponding eigenfrequencies are therefore approximately  $f = nV_A/2S$ , where  $V_A$  is the Alfvén speed near the equator and  $S$  is the length of the field line. Thus, the period of the fundamental mode is the Alfvén bounce period on the field line, while the second harmonic period is half that bounce period. FLRs are commonly observed at Earth, and a large literature exists in which their properties, causes, and consequences have been explored. Recently, *Yates et al.* [2016] showed Cassini magnetic field observations that provide persuasive evidence that field line resonances occur in Saturn's outer magnetosphere and may be responsible for the ~1 h periodicities that have been reported in a number of magnetospheric properties at Saturn, including energetic particle fluxes, magnetic field, plasma wave emissions, and the aurora [see *Palmaerts et al.*, 2016, and references therein]. *Yates et al.* [2016] concluded that their high-latitude magnetic field observations were most consistent with second harmonic Alfvén waves on closed outer magnetospheric field lines with plasma density concentrated near the equator.

Charged particles interacting with the wave fields of FLRs can gain or lose energy depending on the wave phase, the energy distribution of the particles, and spatial gradients in the phase space density. The theoretical basis for such particle energization was explored by *Southwood and Kivelson* [1981, 1982], and recent test particle simulations for conditions at Earth confirm the expected energization [*Rankin et al.*, 2016]. The

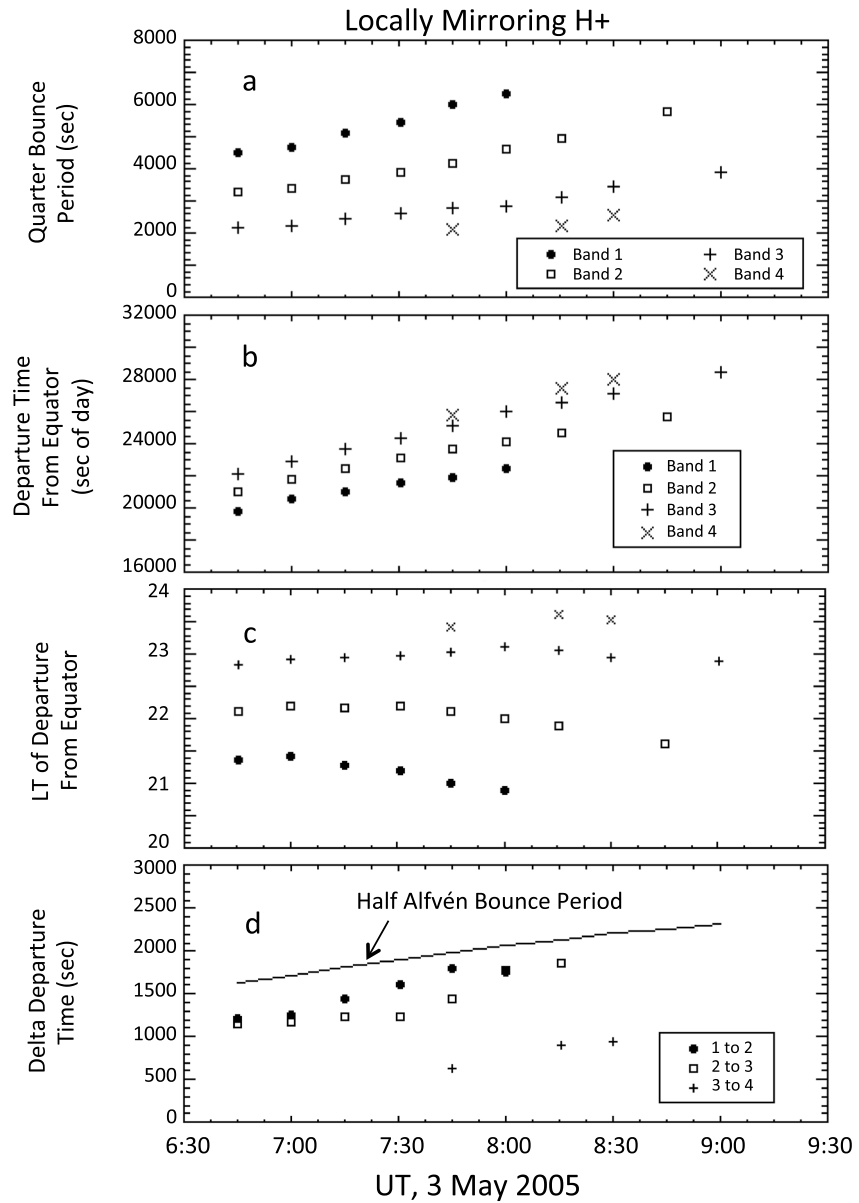


**Figure 7.** (a) Quarter bounce period (i.e., travel time from the equator to the spacecraft) of locally mirroring band particles; (b) time of day (in seconds) at which locally mirroring band particles would have had to leave the equator in order to arrive at the spacecraft at the observation time; (c) local time at which locally mirroring band particles seen at Cassini would have left the equatorial plane, assuming full corotation; and (d) time separation between departure times of successive bands. For comparison, the solid curve shows one half of the bounce period of an Alfvén wave, computed based on the densities and scale heights determined by *Thomsen et al.* [2010]. Band 1 corresponds to the lowest-energy band seen in the ion spectra.

concept has also been successfully applied to particle observations at Earth [e.g., *Yang et al.*, 2010, 2011a, 2011b; *Zong et al.*, 2012; *Ren et al.*, 2016].

In the Southwood and Kivelson analysis, there are two modes of energization: (1) a resonant or near-resonant acceleration/deceleration of particles gradient/curvature drifting parallel to the wave electric field and (2) an adiabatic acceleration/deceleration of particles displaced in  $L$  by  $E \times B$  drifts in the wave electric field. The effect on the flux of particles of a given energy of these two processes can be expressed as

$$\frac{\delta f}{f} = \frac{1}{f} \frac{\partial f}{\partial E} \bigg|_L \Delta E + \frac{1}{f} \frac{\partial f}{\partial L} \bigg|_\mu \Delta L \quad (1)$$

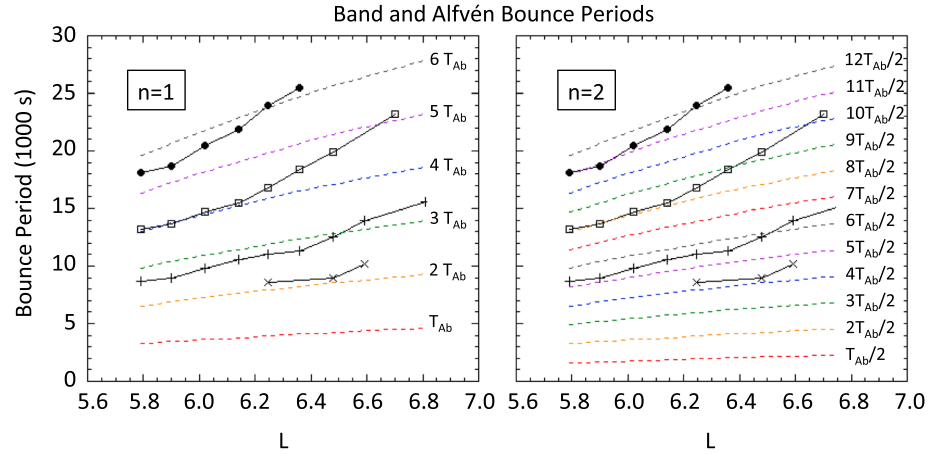


**Figure 8.** Bounce periods of locally mirroring protons at the observed band energies as a function of  $L$ , compared with harmonic multiples of the Alfvén wave bounce period, as expected for the fundamental mode of (left) a field line resonance and (right) the first harmonic.

where

$$\Delta E = qv_D E_\phi \Delta t \quad (2)$$

$$\Delta L = c \frac{E_\phi}{BR_s} \Delta t \quad (3)$$

Here  $f$  is the phase space density of the particle distribution (proportional to flux/energy),  $E$  is the wave electric field,  $v_D$  is the gradient/curvature drift speed of a particle,  $B$  is the ambient (presumed dipole) magnetic field strength,  $R_s$  is the radius of Saturn, and  $\Delta t$  is the time the particle is exposed to the wave.

The energization and radial transport indicated by equations (2) and (3) depend on the sign of the azimuthal component of the electric field [e.g., Southwood and Kivelson, 1981] and in general tend to average to zero as particles bounce in a time-varying field. However, for certain resonant bounce frequencies, the particles repeatedly encounter the wave field in the same orientation, leading to accumulated acceleration (or deceleration). Since the phase space density of the particles decreases with energy, there are more particles available to gain energy than to lose energy, so particles with a resonant bounce frequency will exhibit a flux enhancement over multiple bounces. The resonant bounce periods are integer multiples of the wave period. Hence, for particles interacting with field line resonances, we would expect flux enhancements at energies corresponding to bounce periods of

$$T_b = mT_w = mT_{Ab}/n \quad (4)$$

where  $m$  is the order of the particle resonance,  $n$  is the field line resonant mode number, and  $T_{Ab}$  is the Alfvén wave bounce period.

Figure 8 shows a comparison of the bounce periods computed for locally mirroring protons at the observed band energies and various harmonics of the Alfvén bounce period as given by equation (4) for  $n = 1$  and  $n = 2$ . The Alfvén bounce times were computed as described above. Allowing for uncertainties in the equatorial density distribution and the plasma scale heights, Figure 8 (left) ( $n = 1$ ) shows fairly good agreement between the band ion bounce periods and low orders of the Alfvén bounce period. Figure 8 (right) shows that it would require rather high orders ( $m$ ) to match the observed particle bounce periods in  $n = 2$  and that a number of orders would be missing. However, there are uncertainties in both the equatorial densities and scale heights used above that would probably allow a longer Alfvén bounce period, so we cannot rule out a match for  $n = 2$ . Similarly, even at these relatively low  $L$  values, there is significant field line stretching due to Saturn's ring current, which also tends to increase  $T_{Ab}$ . Thus, we conclude that the band ion bounce periods are consistent with the fundamental or second harmonic FLR.

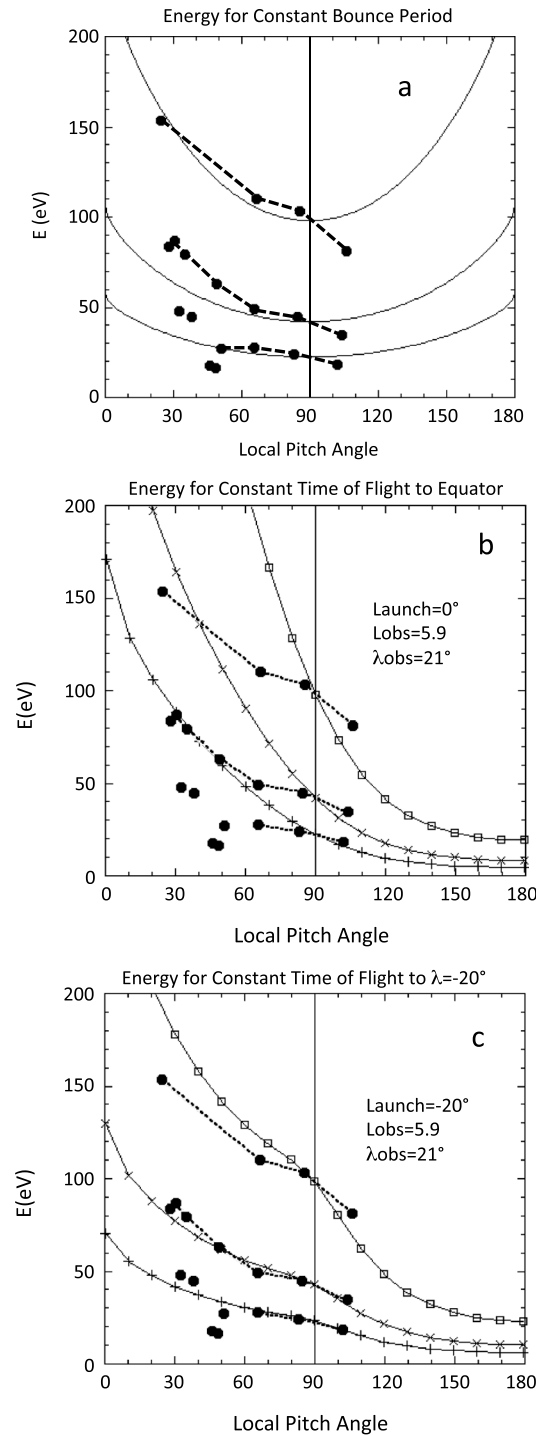


**Figure 9.** Observed band energies (solid circles) as a function of local pitch angle at ~0700 UT, compared to calculated energies for which (a) the bounce periods, (b) the times of flight from the equator, or (c) the times of flight from a latitude of  $-20^\circ$  are equal to those for observed locally mirroring band particles.

of the band energies shown in Figure 6d. While there are clear quantitative discrepancies between the model pitch angle dependence and the observed variation, the qualitative tendency for the band energy to decrease with increasing pitch angle is reproduced.

Assuming a Maxwellian hydrogen distribution with density and temperature as determined by Wilson *et al.* [2008], we can estimate the magnitude of the terms in equation (1). For an Alfvén wave,

$$E_{\phi} = (v_A/c) \cdot \delta B \quad (5)$$

where  $\delta B$  is the magnetic perturbation of the wave, and the equation relates only the amplitudes of the electric and magnetic field perturbations, which are actually orthogonal. Guided by the measurements of Yates *et al.* [2016], we adopt  $\delta B = 0.3$  nT and  $\Delta t = 1800$  s and find that for an H<sup>+</sup> energy of 30 eV at  $L = 6$ , equation (1) gives

$$\frac{\delta f}{f} = 0.009 + 0.018 = 0.027 \quad (6)$$

Thus, a very crude estimate of the effect a field line resonance might have on the hydrogen flux is  $\pm 3\%$  for a single encounter with the wave. Multiple encounters by resonant particles would increase this energization. Given that we do not actually know the wave amplitude encountered by the particles, nor its latitude dependence, this is plausibly close to the value of plus or minus a few to 20% observed between the band peaks and the troughs between them.

### 3.4. Pitch Angle Dependence

One prediction of such a scenario is that the band energies seen at Cassini should vary with pitch angle since it is the parallel component of the particle velocity that determines the bounce frequency. Assuming conservation of particle energy and magnetic moment as ions travel along the magnetic field from the equator to the observation point, one can calculate the energy as a function of local pitch angle for which the bounce periods are equal to those shown for locally mirroring particles in Figure 5a. The result is given in Figure 9a for the CAPS observation at ~0700 UT ( $L \sim 5.9$ ,  $\lambda \sim 21^\circ$ ), overlaid on the observed pitch angle dependence

The one qualitative discrepancy in Figure 9a is that above  $90^\circ$ , the observed band energies continue to decrease, whereas the energies for constant bounce period begin to increase again. This decrease in the band energies across  $90^\circ$  pitch angle is a persistent feature of the banded ions, as shown in Figure 6. As noted above, particles with pitch angles greater than  $90^\circ$  are those that are moving away from the equator, whereas those at pitch angles less than  $90^\circ$  have mirrored at latitudes above the spacecraft and are returning toward the equator. Thus, the particles with pitch angles greater than  $90^\circ$  have traveled a shorter distance since their last equatorial encounter than have particles on the descending part of their bounce (pitch angles less than  $90^\circ$ ). They have also more recently passed through the latitude range below the spacecraft, and it is possible that they have encountered the wave there in a different phase, leading to deceleration rather than acceleration.

On the other hand, the discrepancy in the behavior of the band energy across  $90^\circ$  shown in Figure 9a might be an indication that while the particles are resonant with the wave, what counts most in determining their current state of acceleration/deceleration is the phase of the wave when the particles most recently encountered it. Thus, at any given time the spacecraft will see enhanced fluxes only for particles whose time of flight was such that they encountered the wave region at the right phase; i.e., there will be a discrete energy band corresponding to particles with the right time of flight. This possibility suggests that the bands may correspond to constant times of flight, rather than just constant bounce period. Figure 9b shows the pitch angle dependence of the observed band energies for the same interval as Figure 9a, overlaid on the energy as a function of local pitch angle for which the times of flight from the equator to the spacecraft are equal to those for locally mirroring band particles. Again, there are clear quantitative discrepancies between the model pitch angle dependence and the observed variation, but the qualitative tendency for the band energy to decrease with increasing pitch angle is reproduced, including across  $90^\circ$ .

The agreement between the observed pitch angle dependence of the band energies and the modeled dependence can be improved by changing the presumed origin of the accelerated particles (i.e., the region along the field where the particles encountered large wave amplitudes in the correct direction). Figure 9c shows the same calculation as Figure 9b, except that the ions are assumed to be traveling from a magnetic latitude of  $-20^\circ$ . (Note that in order to yield particles that mirror locally at Cassini, the launch latitude must be less than or equal to the spacecraft latitude.) The energy/pitch angle dispersion in the modeled bands now matches the observations much better than for an equatorial origin.

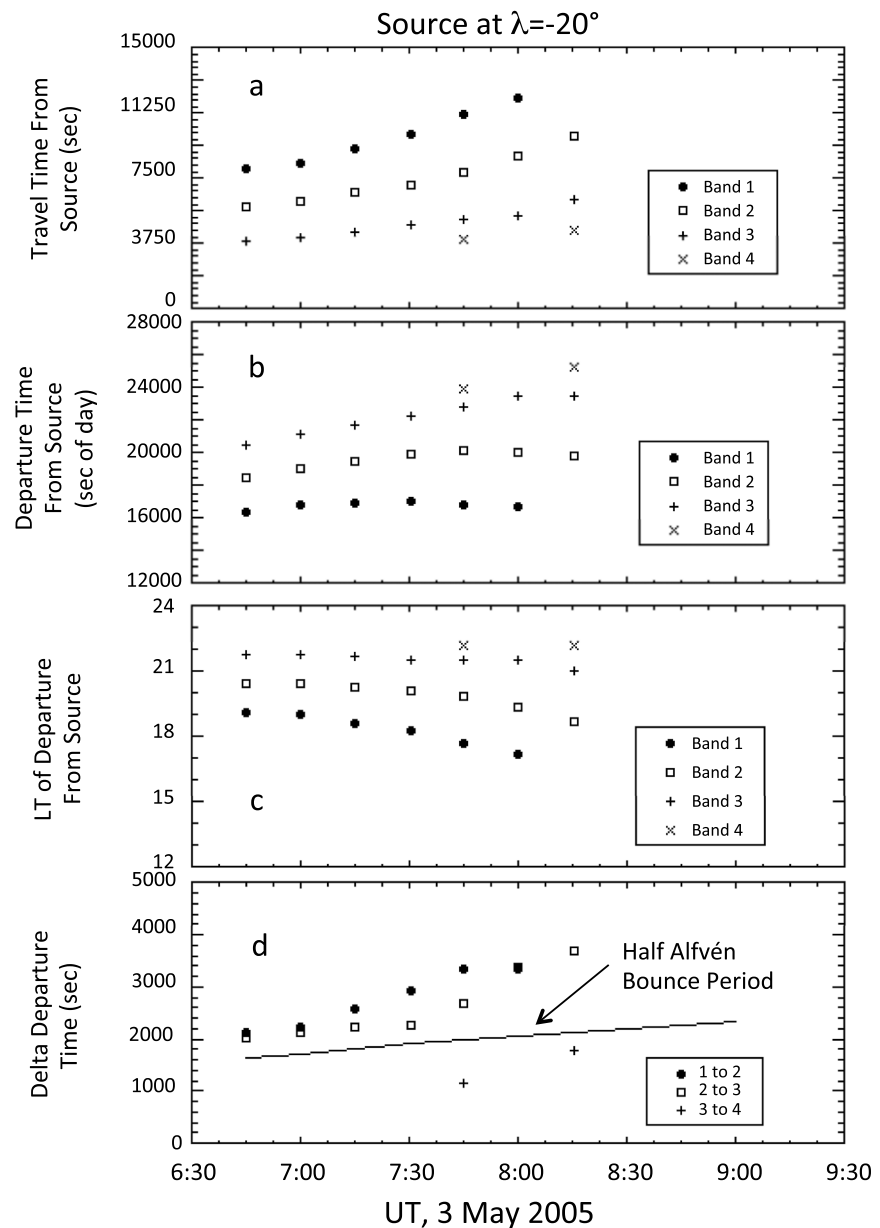
The possibility that the energization of the resonant or near-resonant particles might be dominated by their most recent encounter with the wave is not unreasonable in light of the very long bounce periods of the resonant particles ( $>2$  h, see Figure 7d). To be truly “bounce resonant,” particles would need to encounter the wave on multiple bounces, always in the right wave phase. For such long bounce periods, this would require that the wave properties stay stable over close to a planetary rotation. Thus, any local time dependence to the plasma or field properties would tend to wash out some of the earlier resonant behavior but would leave the most recent wave encounter intact.

Figure 10 is similar to Figure 7 but is constructed under the assumption that the prime acceleration point for the particles was at a latitude of  $-20^\circ$ . From this location, the travel times would be considerably longer, the prime acceleration times considerably earlier ( $\sim 4.6$  UT versus  $\sim 5.7$  UT for an equatorial source), and the local time of origin considerably earlier (near dusk versus  $\sim 21$  LT for an equatorial source). The difference in departure times for the subsequent energy bands is also longer, now somewhat greater than half the Alfvén wave bounce time. We have not attempted to optimize the match to the wave bounce time, but it is clear from Figures 7d and 9d that a source location between the equator and  $\lambda \sim -20^\circ$  would probably bring them fairly close together.

The problem with attributing the bulk of the particle energization to the most recent wave encounter is that the few percent increase in flux estimated above in equation (6) would not be adequate to give the observed flux modulation based on a single wave encounter. To get enough energization in a single encounter, the wave amplitude would have to be much larger than assumed above. Since we do not actually know what the wave amplitude is in the prime acceleration region, we simply leave this as a puzzle for future consideration.

### 3.5. Possible Sources of FLR: Dynamic Pressure Impulse

In the terrestrial magnetosphere, field line resonances not uncommonly originate from a dynamic pressure impulse imparted by the solar wind, such as an interplanetary shock [e.g., *Southwood and Kivelson, 1990; Kivelson and Southwood, 1991*]. The initial impulse propagates through the magnetosphere as a fast-mode



**Figure 10.** Same as Figure 7, except for a source location at  $-20^\circ$  latitude.

compressional wave, which couples to shear mode Alfvén waves that form the field line resonances [e.g., Tamao, 1964; Chen and Hasegawa, 1974; Southwood, 1974; Lysak and Lee, 1992; Chi et al., 2006]. Such conversion occurs primarily in regions of strong gradients of the Alfvén velocity (such as the Earth's plasmopause).

If the banded ions seen by Cassini on 3 May 2005 are due to the passage of a compressional wave front and energization by the standing waves it produces by coupling to a field-aligned wave mode, then we need to ask if there is other observational evidence for the passage of such a compressional wave or the existence of the field line resonance. Figure 11 presents three types of data that are potentially useful for this question: (a) the magnetic field magnitude and azimuthal component measured by Cassini in the hours before and during the banded ion observations [Dougherty et al., 2004]; (b) the electric wave spectra observed by the RPWS instrument during the 2 day interval encompassing the banded ion event, plus 2 day intervals from the previous and subsequent periapsis passes [Gurnett et al., 2004]; and (c) a 50 day interval of solar wind properties projected to Saturn's location via the Michigan Solar Wind Model (mSWIM MHD) model [Zieger and Hansen, 2008].

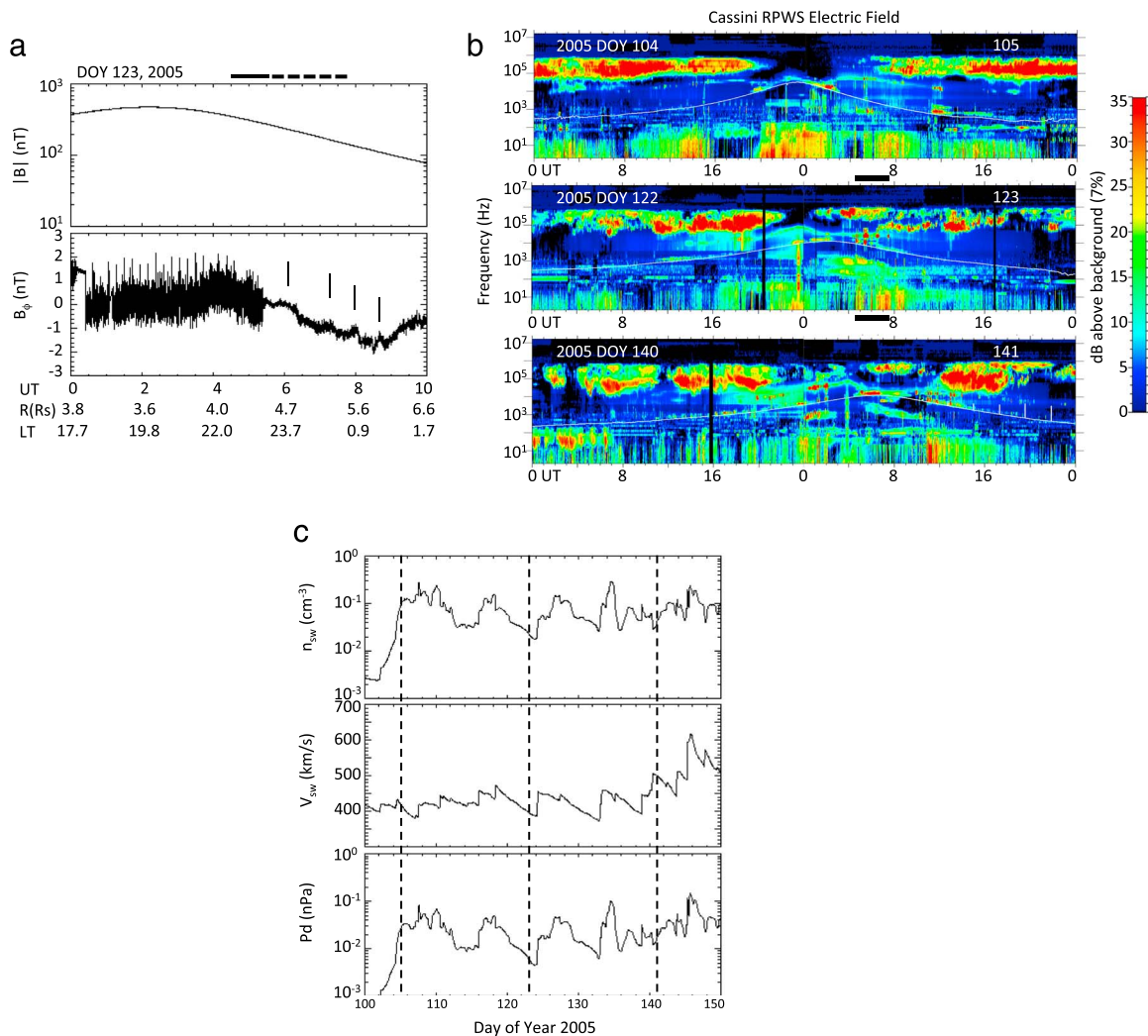


**Figure 11.** (a) Magnetic field magnitude and azimuthal component observed by Cassini for the 10 h encompassing and preceding the banded ion observations. The solid bar above the top panel indicates the range of backward projected departure times of the lowest energy band of ions, both for an assumed equatorial source and for an assumed source at  $-20^\circ$  latitude. If the initial energization of the ions were associated with a compressional wave propagating through the magnetosphere, its signature would presumably occur during this time interval. The dashed bar following the solid bar shows the time range over which subsequent field line resonances would be expected. The vertical bars in the  $B_\phi$  panel indicate semiperiodic enhancements above the background  $B_\phi$ . (b) RPWS electric field spectra for 2 day intervals encompassing three consecutive periapsis passages by Cassini. The outbound passage on which the banded ions were observed is covered in the middle panel. The time interval of the banded ion observation is indicated by the solid bars above and below that panel. (c) Solar wind density, speed, and dynamic pressure at Saturn's location predicted by the mSWIM MHD model [Zieger and Hansen, 2008] for a 50 d interval encompassing the three periapsis passes shown in Figure 11b (vertical dashed lines).

In Figure 11a, the interval corresponding to the backward projected departure times of the lowest energy band of ions is shown as the solid black bar above the panel. The range of this bar covers the range of ion departure times both for an assumed equatorial encounter with the wave and one at  $-20^\circ$  latitude, and any passing compressional wave would presumably be found somewhere near this time. The dashed bar just to the right of the solid bar indicates the range of times over which field line resonances would be expected.

Examination of the top panel of Figure 11a reveals no indication of a magnetic field compression occurring near the solid bar or any other time during the 10 h interval displayed. Subtraction of a dipole model to examine residual field (not shown) also does not show significant evidence of compression. Any variations in the field strength are at less than the 1% level throughout. Magnetic compression signatures have previously been reported in Saturn's lobes [e.g., Jackman et al., 2010; Thomsen et al., 2015] but not within the inner magnetosphere (other than those associated with interchange injection events). However, observations of compressional pulses launched into Earth's magnetosphere suggest at least three possible considerations

that might make it difficult to detect compressions at Cassini's location at this time: The first is that Cassini was located near midnight local time during the interval when a compressional signal might have been propagating through the region (cf. Figure 11a), and numerous studies at the Earth (particularly at geosynchronous orbit,  $L = 6.6$ ) have shown that the geomagnetic field response to sharp solar wind dynamic pressure variations is typically very weak to nonexistent on the nightside [e.g., Borodkova *et al.*, 2005; Wang *et al.*, 2007; Villante and Piersanti, 2008; Jackel *et al.*, 2012]. The second consideration is that Cassini was at very low  $L$  values ( $\sim 4$ ) at the time a compression might have been expected. Since the magnetic field there is quite large, one might not expect to observe a significant compressional signature. Finally, the third consideration is that Cassini was also at a relatively high latitude ( $\sim 20^\circ$ ); information about the latitude dependence of the compressional signals at Earth does not seem to be available in the literature (except at ionospheric altitudes), but it seems possible that the compressional signature may be largely confined to the near-equatorial region. Moreover, measurements from a global MHD simulation of Saturn's magnetospheric response to a solar wind dynamic pressure enhancement [Jia *et al.*, 2012] show a compressive signal less than 1% of the ambient magnetospheric magnetic field at  $L = 6$ ,  $LT = 23$  and latitude =  $20^\circ$  (X. Jia, unpublished analysis). The small amplitude of the signature, combined with the decreasing relative amplitude as the background field increases between  $L = 6$  and  $L = 4$ , suggests that Cassini may well not have been able to detect a tiny compression this deep in the magnetosphere at a latitude of  $20^\circ$ .

The bottom panel in Figure 11a shows the azimuthal component of the magnetic field observed at Cassini through this time period. High-frequency fluctuations visible in the figure after  $\sim 05:30$  UT may be electromagnetic ion cyclotron waves, which are ubiquitous in the ion pickup region of Saturn's inner magnetosphere [e.g., Leisner *et al.*, 2006; Russell *et al.*, 2006]. Between about 00:30 and 05:30 UT the instrument was operating in a higher dynamic range, and the interval of sharply higher fluctuation amplitudes then is due to the digitization level in that range. In addition to these high-frequency signals, there are three to four enhancements in  $B_\phi$  separated by  $\sim 40$  min, as indicated by the vertical bars in the panel. It seems possible that these could be the signature of the field line resonances left behind on these field lines by the passage of a compressional signal at an earlier local time (closer to 18 LT, see Figure 9).

While the magnetic field data of Figure 11a do not show any direct evidence of the occurrence of a sudden compression of the magnetosphere, we can also look for a signature in the observations of the RPWS instrument. Previous work has shown that solar wind dynamic pressure enhancements characteristically lead to sudden brightenings of Saturn Kilometric Radiation (SKR) emissions and the extension of SKR to lower frequencies than its normal range [e.g., Desch, 1982; Kurth *et al.*, 2005; Bunce *et al.*, 2005; Mitchell *et al.*, 2005; Jackman *et al.*, 2009, 2010; Thomsen *et al.*, 2015]. Figure 11b presents RPWS electric field spectra for the 2 days surrounding the periapsis pass on which the banded ions were seen (marked by the solid bars above and below the middle panel), as well as the 2 day intervals surrounding the two periapsis passes immediately preceding and following the one of interest here (top and bottom panels). In these spectrograms, SKR emissions are seen as wave power above a few tens of kilohertz, except in a "shadow zone" near periapsis where such waves are excluded [e.g., Galopeau *et al.*, 1989; Lamy *et al.*, 2008]. In comparing the inbound versus outbound RPWS observations surrounding periapsis on day 123 (Figure 11b, middle panel), we find no evidence for an enhancement in SKR intensity, nor an extension to lower frequencies, during the time when our analysis above would predict the passage of the compressional wave (approximately a few hours after midnight on day 123). Indeed, comparison of the middle panel in Figure 11b with the top and bottom panels does not reveal any distinctive plasma wave signature that might be attributed to the passage of a solar wind dynamic pressure enhancement on day 123. There exists a possibility that if the SKR during the interval of interest was dominantly from the southern source, the so-called shadow zone [Lamy *et al.*, 2008] might have prevented Cassini at relatively high northern latitudes from seeing the emissions, but this should not have affected SKR observations beyond  $L \sim 7$ . Thus, SKR data do not appear to support the occurrence of a global compression early on day 123.

Finally, Figure 11c explores the possibility of a solar wind dynamic pressure increase by reference to the solar wind parameters predicted at Saturn's orbit by the MHD model mSWIM, constrained by 1 AU observations [Zieger and Hansen, 2008]. Figure 11c presents the predicted density, speed, and dynamic pressure at Saturn's location between day 100 and day 150 of 2005. The three periapsis intervals shown in Figure 11b are indicated by the vertical dashed lines. The model predicts that early on day 123 Saturn would have been in the low-speed, low-density rarefaction region preceding the arrival of a high-speed stream early on day

124. The year 2005 was a good one for mSWIM predictions in that it featured a high recurrence index of solar wind properties [Zieger and Hansen, 2008], but unfortunately, the interval of interest around day 123 was quite far removed from the optimum near opposition of Earth and Saturn, for which the model predictions are most accurate (days 13–41 in 2005 (mSWIM webpage <http://mswim.engin.umich.edu/validation.php>)). In Zieger and Hansen's, 2008 study, for intervals  $\sim 100$  days after near opposition, there is considerable uncertainty in the modeled shock arrival time, with both positive and negative time lags (prediction later/earlier than actual arrival, respectively) up to 40 h or so. Thus, it is possible that the shock predicted by mSWIM on day 124 could have arrived early on day 123 at the time expected according to the hypothesis we have advanced. RPWS saw no strong enhancement of SKR or any low-frequency extensions on day 124 (not shown), suggesting that the predicted pressure enhancement did not arrive on that day.

In summary, we find possible evidence for a field line resonance in a few  $B_p$  enhancements seen in the same time frame as the banded ions, with time separations  $\sim 40$  min, comparable to 0.5–1 times the Alfvén bounce period (cf. Figure 10d). However, while the mSWIM model predicts a solar wind dynamic pressure enhancement on the following day, which would be within the uncertainty of the modeling, the observations in Figure 11 provide no clear magnetospheric evidence supporting the passage of a global compressional event early on day 123. Nonetheless, because compressional waves propagate in all directions relative to  $B$ , compressional perturbations are so spatially dispersed that even a small amplitude compression can have a significant effect on a global scale. A resonant flux tube extracts energy all along its extent from ionosphere to ionosphere and the locally small compressional perturbations can thus be a significant energy source for the standing wave resonance. So we cannot fully rule out the possibility of a solar wind impulse as the stimulus for the FLR.

### 3.6. Possible Sources of FLR: Magnetopause Fluctuations

Another possible source for the inferred field line resonances is the ongoing Kelvin-Helmholtz (KH) activity at the magnetopause or pulsed magnetopause reconnection, as have been found at Earth [e.g., Singer et al., 1977; Anderson et al., 1991; Engebretson et al., 1998; Le et al., 2004]. Evidence for KH waves at Saturn's magnetopause has certainly been reported in Cassini in situ data [e.g., Masters et al., 2009, 2010, 2012; Cutler et al., 2011; Wilson et al., 2012] and in small-scale structure in auroral emissions [Grodent et al., 2011]. A survey of magnetic signatures of KH at Saturn found that the occurrence frequency is highest on the dusk flank, contrary to previous expectations [Delamere et al., 2013], but subsequent theoretical exploration of the KH instability at Saturn confirmed that the dusk magnetopause should often be KH unstable and that KH is inhibited on the dawnside [Desroche et al., 2013]. The banded-ion observations presented here seem to imply field line resonances on the dusk side, consistent with this dusk preference for KH.

A number of recent Cassini observations have reported quasi-periodic variations with periods  $\sim 1$  h in magnetospheric properties, especially the fluxes of energetic particles, auroral broadening, auroral hiss, and the magnetic field [Roussos et al., 2016; Mitchell et al., 2016; Palmaerts et al., 2016; Yates et al., 2016]. The statistical occurrence of the quasi-periodic phenomena suggests a high-latitude source [Palmaerts et al., 2016], and several authors have suggested that they originate in KH instability of the magnetopause [Roussos et al., 2016; Mitchell et al., 2016]. Thus, it seems possible that KH waves at the magnetopause, especially at dusk, could drive field line resonances throughout the dusk magnetosphere.

### 3.7. Possible Sources of FLR: Planetary Period Oscillations

Finally, as mentioned above, Yates et al. [2016] have presented high-latitude observations of  $\sim 1$  h periodicities in the magnetic field, primarily transverse to the average field. They have identified these fluctuations as second harmonic Alfvén waves standing on closed outer-magnetospheric field lines. The fluctuations analyzed by Yates et al. persisted for 6 days, from day 338 (4 December) through day 343 (9 December) of 2006. From Table 2 we note that one of the banded-ion events we have found occurred on the day preceding the Yates interval, while Cassini was outbound through the inner magnetosphere. This close proximity in time provides yet another link between banded ions and FLRs. Further, the long duration of the Yates interval suggests that stimulation of the waves by a passing solar wind dynamic pressure enhancement is unlikely.

Most intriguingly, Yates et al. [2016] found that the 1 h magnetic fluctuations were temporally modulated, occurring in wave packets that in the Northern Hemisphere recur periodically at the northern magnetic oscillation period [e.g., Gurnett et al., 2009, 2011; Andrews et al., 2012; Provan et al., 2012]. They attributed the wave

packet structure to a rocking of the magnetosphere due to whatever dynamical process is responsible for the much studied planetary period oscillations (PPO) (see *Carbary and Mitchell* [2013] for a review of PPO observations and models and *Cowley et al.* [2016a] for a recent update). As for the source of the Alfvén waves themselves, *Yates et al.* [2016] suggested that they “are probably generated by some dynamical process occurring in the outer magnetosphere or in the central plasma sheet.”

The PPOs observed in magnetic field measurements have been very successfully modeled by a dual corotating field-aligned current system [e.g., *Southwood and Kivelson*, 2007; *Andrews et al.*, 2010, 2012; *Provan et al.*, 2012; *Cowley et al.*, 2016b]. These field-aligned currents emerge naturally from the atmospheric vortex model of PPOs, which imposes a rotating pattern of flow in the ionosphere that results in periodic modulation of the magnetosphere-ionosphere coupling currents [*Jia et al.*, 2012; *Jia and Kivelson*, 2012]. While it is well beyond the scope of this paper to investigate the possibility, we offer the speculation that it may be these time-varying field-aligned currents associated with the planetary period oscillations that periodically power the Alfvén waves that form the field line resonances in the magnetosphere. *Kivelson and Jia* [2014] showed how compressional fronts are launched by these ionospheric current sources of planetary period oscillations. Since any compressional disturbance has the possibility of coupling into a field line resonance, generation of FLRs might be a nearly continuous process, modulated at the planetary period.

Such an internal source would account for the wide distribution of  $\sim 1$  h periodic phenomena throughout Saturn’s magnetosphere. In particular, field line resonances would not be confined to the outer magnetosphere but could potentially be produced in the inner magnetosphere where we observe the banded ions. Moreover, FLRs would be expected to be a rather common occurrence throughout the magnetosphere, not requiring the relatively infrequent dynamic pressure events in the solar wind, nor any particular KH activity at the magnetopause. Indeed, as pointed out above, the *Yates et al.* observations showed the 1 h waves persisting for at least 6 days, which is quite unlikely for FLRs created by a single solar wind pressure pulse. Further, this would require relatively stable solar wind properties over that timescale if Kelvin-Helmholtz waves are to be the source, but such long intervals would easily be consistent with a repeating internal source.

#### 4. Summary

1. On 3 May 2005 (day 123) the cool ion distribution observed by Cassini exhibited approximately three to four discrete bands in  $E/q$ . The band energies uniformly decreased with increasing radial distance, but they appeared superimposed on a background thermal population that followed the expected general increase with  $r$ .
2. The banded ions were a globally coherent feature, lasting at least  $\sim 4$  h, and covering at least the  $L$  range from 5.7 to 7.5, the local time region from pre-midnight to  $\sim 2$  LT, and  $\sim 106^\circ$  of SLS2 longitude [e.g., *Kurth et al.*, 2007].
3. The fact that the energy flux was larger for particles coming from the equator than for particles coming from high latitudes points to a more equatorial source of the population or possibly one in the Southern Hemisphere.
4. The energy of the bands appeared to decrease with increasing pitch angle, even across  $90^\circ$ .
5. The bands that CAPS saw were dominantly  $H^+$ , and we are unable to determine whether or not the heavier species ( $H_2^+$  and  $W^+$ ) were similarly banded, preventing the type of species comparisons (e.g., common energy or common time of flight) that have proven valuable at Earth [e.g., *Colpitts et al.*, 2016].
6. Projecting backward in time, the banded ions seen by Cassini would have departed the equator in the pre-midnight region  $\sim 0.5$ – $1.5$  h prior to their observation (the shorter travel times corresponding to the higher-energy bands). The times between the projected departures of the various energy bands would have been  $\sim 1000$ – $2000$  s, comparable to the estimated half bounce period of Alfvén waves on these field lines. Departure from a southern magnetic latitude of  $20^\circ$  rather than the equator would have resulted in roughly twice that travel time and twice the difference times, but again, the difference times would be comparable to the Alfvén wave half bounce period.
7. We hypothesize that the banded ions are formed by a bounce-resonant interaction between magnetospheric  $H^+$  ions and the standing wave structure of a field line resonance. The observed band energies are consistent with the expectation that the bounce period of resonant particles would be related to the Alfvén bounce period by equation (4). For the plasma and field parameters we have adopted for

the calculation, the  $n = 1$  FLR (with a peak wave amplitude near the equator) seems to provide a better match to the band energies in that it allows a frequency match for relatively low orders of the bounce resonance ( $m = 1, 2, \dots$ ), but with reasonable variations of the plasma and field properties, the  $n = 2$  FLR might also give a satisfactory match.

8. The pitch angle dependence of the band energies is generally consistent with the bounce resonance hypothesis, except that the band energies decrease rather than increase with pitch angle above  $90^\circ$ . This feature is robust throughout much of the interval of the bands. It may indicate that these particles, which are traveling away from the equatorial plane, have been less effectively accelerated during their interaction with the wave. Alternatively, we raise the possibility that the banded ions all encountered the wave most recently when and where it was at its most effective magnitude and direction for ion acceleration, so that they share a common time of flight from that region. This hypothesis reproduces well the pitch angle dependence of the band energies, including the continued decrease across  $90^\circ$ , especially if the effective acceleration region is taken to be at  $-20^\circ$  latitude.
9. Estimates of the amplitude of flux modulation that might be expected from interaction of magnetospheric plasma with FLRs are plausibly in range of the observed flux variations in the bands.
10. One possible source of such FLRs is the coupling of a fast-mode compressional wave propagating through the inner magnetosphere, perhaps as the magnetospheric response to a sudden solar wind dynamic pressure enhancement. However, we find no evidence in the magnetic field or SKR observations to support the occurrence of such a large-scale compression in the required time frame, although we do find possible evidence for the magnetic fluctuations arising from a field line resonance.
11. Other possible FLR sources might be Kelvin-Helmholtz waves generated at the magnetopause or possibly the variable field-aligned current system and compressional disturbances associated with planetary period oscillations.

## 5. Conclusion

While energy-banded ions are observed not uncommonly in Earth's magnetosphere, we have reported here the first observation of banded ions at Saturn. Observed near midnight at relatively high magnetic latitudes within the inner magnetosphere, the banded ions are dominantly  $H^+$ , and they occupy the range of energies typically associated with the thermal pickup distribution in the inner magnetosphere. The observed energies of the bands, including their pitch angle variation, are consistent with a bounce-resonant interaction between thermal  $H^+$  ions and the standing wave structure of a field line resonance. There is evidence in the pitch angle dependence of the band energies that the particles in each band may have a common time of flight from their most recent interaction with the wave, which may have been at slightly southern latitudes. While it is beyond the scope of this paper to determine definitively the process(es) producing these energy bands, we hope that it will stimulate further attention to mechanisms of thermal ion acceleration in Saturn's magnetosphere, as well as studies of field line resonances there.

## References

- Anderson, B. J., T. A. Potemra, L. J. Zanetti, and M. J. Engebretson (1991), Statistical correlations between Pc3–5 pulsations and solar wind/IMF parameters and geomagnetic indices, in *Physics of Space Plasmas (1990)*, *SPI Conf. Proc. Reprint Ser.*, vol. 10, edited by T. Chang et al., pp. 419–429, Scientific, Cambridge, Mass.
- Andrews, D. J., A. J. Coates, S. W. H. Cowley, M. K. Dougherty, L. Lamy, G. Provan, and P. Zarka (2010), Magnetospheric period oscillations at Saturn: Comparison of equatorial and high latitude magnetic field periods with north and south Saturn kilometric radiation periods, *J. Geophys. Res.*, *115*, A12252, doi:10.1029/2010JA015666.
- Andrews, D. J., S. W. H. Cowley, M. K. Dougherty, L. Lamy, G. Provan, and D. J. Southwood (2012), Planetary period oscillations in Saturn's magnetosphere: Evolution of magnetic oscillation properties from southern summer to post-equinox, *J. Geophys. Res.*, *117*, A04224, doi:10.1029/2011JA017444.
- Borodkova, N., G. Zastenker, M. Riazantseva, and J. Richardson (2005), Large and sharp solar wind dynamic pressure variations as a source of geomagnetic field disturbances at the geosynchronous orbit, *Planet. Space Sci.*, *53*, 25–32, doi:10.1016/j.pss.2004.09.025.
- Bridge, H. S., et al. (1981), Plasma observations near Saturn: Initial results from Voyager 1, *Science*, *212*, 217–224, doi:10.1126/science.212.4491.217.
- Bunce, E. J., S. W. H. Cowley, D. M. Wright, A. J. Coates, M. K. Dougherty, N. Krupp, W. S. Kurth, and A. M. Rymer (2005), In situ observations of a solar wind compression-induced hot plasma injection in Saturn's tail, *Geophys. Res. Lett.*, *32*, L20504, doi:10.1029/2005GL022888.
- Burch, J. L., J. Goldstein, T. W. Hill, D. T. Young, F. J. Crary, A. J. Coates, N. André, W. S. Kurth, and E. C. Sittler Jr. (2005), Properties of local plasma injections in Saturn's magnetosphere, *Geophys. Res. Lett.*, *32*, L14502, doi:10.1029/2005GL022611.
- Burton, M. E., M. K. Dougherty, and C. T. Russell (2010), Saturn's internal planetary magnetic field, *Geophys. Res. Lett.*, *37*, L24105, doi:10.1029/2010GL045148.
- Carbary, J. F., and D. G. Mitchell (2013), Periodicities in Saturn's magnetosphere, *Rev. Geophys.*, *51*, 1–30, doi:10.1002/rog.20006.

## Acknowledgments

This work benefited greatly from collaborative discussions that took place during a visit of MFT to the University of Southampton as a Diamond Jubilee fellow. The support provided by the Diamond Jubilee Fellowship is gratefully acknowledged. Work at PSI was supported by the NASA Cassini program through JPL contract 1243218 with Southwest Research Institute. The Cassini project is managed by the Jet Propulsion Laboratory for NASA. S.V.B. is supported by STFC Ernest Rutherford Fellowship ST/M005534/1. C. M.J. is supported by a Science and Technology Facilities Council Ernest Rutherford Fellowship ST/L004399/1. M. G.K. is supported by NASA grant NNX14AG87G:000002. The research at the University of Iowa was supported by NASA through contract 1415150 with the Jet Propulsion Laboratory. Work by X.J. is supported by NASA grant NNX15AH28G. All Cassini plasma, magnetometer, and plasma wave data used for this study are available from the Planetary Data System (<http://pds.nasa.gov/>). We thank K.C. Hansen and B. Zieger for providing solar wind propagations from their Michigan Solar Wind Model (<http://mswim.engin.umich.edu/>).

- Chen, L., and A. Hasegawa (1974), A theory of long-period magnetic pulsations: 1. Steady state excitation of field line resonance, *J. Geophys. Res.*, **79**(7), 1024–1032, doi:10.1029/JA079i007p01024.
- Chi, P. J., D.-H. Lee, and C. T. Russell (2006), Tamao travel time of sudden impulses and its relationship to ionospheric convection vortices, *J. Geophys. Res.*, **111**, A08205, doi:10.1029/2005JA011578.
- Colpitts, C. A., C. A. Cattell, J. U. Kozyra, M. F. Thomsen, and B. Lavraud (2016), Satellite observations of energy-banded ions during large geomagnetic storms: Event studies, statistics, and comparisons to source models, *J. Geophys. Res. Space Physics*, **121**, 6353–6377, doi:10.1002/2016JA022481.
- Cowley, S. W. H., P. Zarka, G. Provan, L. Lamy, and D. J. Andrews (2016a), Comment on “A new approach to Saturn’s periodicities” by J. F. Carbary, *J. Geophys. Res. Space Physics*, **121**, 2418–2422, doi:10.1002/2015JA021996.
- Cowley, S. W. H., G. Provan, G. J. Hunt, and C. M. Jackman (2016b), Planetary period modulations of Saturn’s magnetotail current sheet: A simple illustrative mathematical model, *J. Geophys. Res. Space Physics*, **121**, 258–279, doi:10.1002/2016JA023367.
- Cutler, J. C., M. K. Dougherty, E. A. Lucek, and A. Masters (2011), Evidence of surface wave on the dusk flank of Saturn’s magnetopause possibly caused by the Kelvin–Helmholtz instability, *J. Geophys. Res.*, **116**, A10220, doi:10.1029/2011JA016643.
- Delamere, P. A., R. J. Wilson, S. Eriksson, and F. Bagenal (2013), Magnetic signatures of Kelvin–Helmholtz vortices on Saturn’s magnetopause: Global survey, *J. Geophys. Res. Space Physics*, **118**, 393–404, doi:10.1029/2012JA018197.
- Desch, M. D. (1982), Evidence for solar wind control of Saturn radio emission, *J. Geophys. Res.*, **87**(A6), 4549–4554, doi:10.1029/JA087iA06p04549.
- Desroche, M., F. Bagenal, P. A. Delamere, and N. Erkaev (2013), Conditions at the magnetopause of Saturn and implications for the solar wind interaction, *J. Geophys. Res. Space Physics*, **118**, 3087–3095, doi:10.1002/jgra.50294.
- Dougherty, M. K., et al. (2004), The Cassini magnetic field investigation, *Space Sci. Rev.*, **114**, 331–383.
- Engelbreton, M. J., K.-H. Glassmeier, and M. Stellmacher (1998), The dependence of high-latitude Pc5 power on solar wind velocity and phase of high-speed solar wind streams, *J. Geophys. Res.*, **103**, 26,271–26,283, doi:10.1029/97JA03143.
- Galozeau, P., P. Zarka, and D. Le Quéau (1989), Theoretical model of Saturn’s kilometric radiation spectrum, *J. Geophys. Res.*, **94**(A7), 8739–8755, doi:10.1029/JA094iA07p08739.
- Grodent, D., J. Gustin, J. C. Gerard, A. Radioti, B. Bonfond, and W. R. Pryor (2011), Small-scale structures in Saturn’s ultraviolet aurora, *J. Geophys. Res.*, **116**, A09225, doi:10.1029/2011JA016818.
- Gurnett, D. A., et al. (2004), The Cassini radio and plasma wave investigation, *Space Sci. Rev.*, **114**, 395–463.
- Gurnett, D. A., A. Lecacheux, W. S. Kurth, A. M. Persoon, J. B. Groene, L. Lamy, P. Zarka, and J. F. Carbary (2009), Discovery of a north-south asymmetry in Saturn’s radio rotation period, *Geophys. Res. Lett.*, **36**, L16102, doi:10.1029/2009GL039621.
- Gurnett, D. A., J. B. Groene, T. F. Averkamp, W. S. Kurth, S.-Y. Ye, and G. Fischer (2011), The SLS4 longitude system based on a tracking filter analysis of the rotational modulation of Saturn kilometric radiation, in *Planetary Radio Emissions VII*, edited by H. O. Rucker et al., pp. 51–64, Austrian Acad. Sci. Press, Vienna.
- Hill, T. W., A. M. Rymer, J. L. Burch, F. J. Crary, D. T. Young, M. F. Thomsen, D. Delapp, N. André, A. J. Coates, and G. R. Lewis (2005), Evidence for rotationally driven plasma transport in Saturn’s magnetosphere, *Geophys. Res. Lett.*, **32**, L14510, doi:10.1029/2005GL022620.
- Holmberg, M. K. G., J.-E. Wahlund, M. W. Morooka, and A. M. Persoon (2012), Ion densities and velocities in the inner plasma torus of Saturn, *Planet. Space Sci.*, **73**, 151, doi:10.1016/j.pss.2012.09.016.
- Hughes, W. J. (1994), Magnetospheric, ULF waves: A tutorial with a historical perspective, in *Solar Wind Sources of Magnetospheric Ultra-Low-Frequency Waves*, pp. 1–11, AGU, Washington, D. C.
- Jackel, B. J., B. McKiernan, and H. J. Singer (2012), Geostationary magnetic field response to solar wind pressure variations: Time delay and local time variation, *J. Geophys. Res.*, **117**, A05203, doi:10.1029/2011JA017210.
- Jackman, C. M., L. Lamy, M. P. Freeman, P. Zarka, B. Cecconi, W. S. Kurth, S. W. H. Cowley, and M. K. Dougherty (2009), On the character and distribution of lower-frequency radio emissions at Saturn and their relationship to substorm-like events, *J. Geophys. Res.*, **114**, A08211, doi:10.1029/2008JA013997.
- Jackman, C. M., C. S. Arridge, J. A. Slavin, S. E. Milan, L. Lamy, M. K. Dougherty, and A. J. Coates (2010), In situ observations of the effect of a solar wind compression on Saturn’s magnetotail, *J. Geophys. Res.*, **115**, A10240, doi:10.1029/2010JA015312.
- Jia, X., and M. G. Kivelson (2012), Driving Saturn’s magnetospheric periodicities from the upper atmosphere/ionosphere: Magnetotail response to dual sources, *J. Geophys. Res.*, **117**, A11219, doi:10.1029/2012JA018183.
- Jia, X., K. C. Hansen, T. I. Gombosi, M. G. Kivelson, G. Tóth, D. L. DeZeeuw, and A. J. Ridley (2012), Magnetospheric configuration and dynamics of Saturn’s magnetosphere: A global MHD simulation, *J. Geophys. Res.*, **117**, A05225, doi:10.1029/2012JA017575.
- Kivelson, M. G., and X. Jia (2014), Control of periodic variations in Saturn’s magnetosphere by compressional waves, *J. Geophys. Res. Space Physics*, **119**, 8030–8045, doi:10.1002/2014JA020258.
- Kivelson, M. G., and D. J. Southwood (1985), Resonant ULF waves: A new interpretation, *Geophys. Res. Lett.*, **12**, 49–52, doi:10.1029/GL012i001p00049.
- Kivelson, M. G., and D. J. Southwood (1991), Ionospheric traveling vortex generation by solar wind buffeting of the magnetosphere, *J. Geophys. Res.*, **96**(A2), 1661–1667, doi:10.1029/90JA01805.
- Kurth, W. S., G. B. Hospodarsky, D. A. Gurnett, B. Cecconi, P. Louarn, A. Lecacheux, P. Zarka, H. O. Rucker, M. Boudjada, and M. L. Kaiser (2005), High spectral and temporal resolution observations of Saturn kilometric radiation, *Geophys. Res. Lett.*, **32**, L20507, doi:10.1029/2005GL022648.
- Kurth, W. S., A. Lecacheux, T. F. Averkamp, J. B. Groene, and D. A. Gurnett (2007), A Saturnian longitude system based on a variable kilometric radiation period, *Geophys. Res. Lett.*, **34**, L02201, doi:10.1029/2006GL028336.
- Lamy, L., P. Zarka, B. Cecconi, S. Hess, and R. Prangé (2008), Modeling of Saturn kilometric radiation arcs and equatorial shadow zone, *J. Geophys. Res.*, **113**, A10213, doi:10.1029/2008JA013464.
- Le, G., et al. (2004), Coordinated polar spacecraft, geosynchronous spacecraft, and ground-based observations of magnetopause processes and their coupling to the ionosphere, *Ann. Geophys.*, **22**, 4329–4350, doi:10.5194/angeo-22-4329-2004.
- Leisner, J. S., C. T. Russell, M. K. Dougherty, X. Blanco-Cano, R. J. Strangeway, and C. Bertucci (2006), Ion cyclotron waves in Saturn’s E ring: Initial Cassini observations, *Geophys. Res. Lett.*, **33**, L11101, doi:10.1029/2005GL024875.
- Livi, R., J. Goldstein, J. L. Burch, F. Crary, A. M. Rymer, D. G. Mitchell, and A. M. Persoon (2014), Multi-instrument analysis of plasma parameters in Saturn’s equatorial, inner magnetosphere using corrections for spacecraft potential and penetrating background radiation, *J. Geophys. Res. Space Physics*, **119**, 3683–3707, doi:10.1002/2013JA019616.
- Lysak, R. L., and D. H. Lee (1992), Response of the dipole magnetosphere to pressure pulses, *Geophys. Res. Lett.*, **19**, 937–940, doi:10.1029/92GL00625.
- Masters, A., N. Achilleos, C. Bertucci, M. K. Dougherty, S. J. Kanani, C. S. Arridge, H. J. McAndrews, and A. J. Coates (2009), Surface waves on Saturn’s dawn flank magnetopause driven by the Kelvin–Helmholtz instability, *Planet. Space Sci.*, **57**, 1769.
- Masters, A., et al. (2010), Cassini observations of a Kelvin–Helmholtz vortex in Saturn’s outer magnetosphere, *J. Geophys. Res.*, **115**, A07225, doi:10.1029/2010JA015351.

- Masters, A., N. Achilleos, J. C. Cutler, A. J. Coates, M. K. Dougherty, and G. H. Jones (2012), Surface waves on Saturn's magnetopause, *Planet. Space Sci.*, *65*, 109, doi:10.1016/j.pss.2012.02.007.
- Mitchell, D. G., et al. (2005), Energetic ion acceleration in Saturn's magnetotail: Substorms at Saturn?, *Geophys. Res. Lett.*, *32*, L20S01, doi:10.1029/2005GL022647.
- Mitchell, D. G., J. F. Carbary, E. J. Bunce, A. Radioti, S. V. Badman, W. R. Pryor, G. B. Hospodarsky, and W. S. Kurth (2016), Recurrent pulsations in Saturn's high latitude magnetosphere, *Icarus*, *263*, 94, doi:10.1016/j.icarus.2014.10.028.
- Palmaerts, B., E. Roussos, N. Krupp, W. S. Kurth, D. G. Mitchell, and J. N. Yates (2016), Statistical analysis and multi-instrument overview of the quasi-periodic 1-hour pulsations in Saturn's outer magnetosphere, *Icarus*, *271*, 1, doi:10.1016/j.icarus.2016.01.025.
- Porco, C. C., et al. (2006), Cassini observes the active south pole of Enceladus, *Science*, *311*, 1393–1401, doi:10.1126/science.1123013.
- Provan, G., D. J. Andrews, C. S. Arridge, A. J. Coates, S. W. H. Cowley, G. Cox, M. K. Dougherty, and C. M. Jackman (2012), Dual periodicities in planetary-period magnetic field oscillations in Saturn's tail, *J. Geophys. Res.*, *117*, A01209, doi:10.1029/2011JA017104.
- Rankin, R., C. Wang, D. Sydorenko, Y. Wang, Q.-G. Zong, and X. Zhou (2016), Simulation of bounce-resonance ULF wave-particle interactions, 2016 URSI Asia-Pacific Radio Sci. Conf. (URSI AP-RASC), pp. 956–959.
- Ren, J., Q. G. Zong, X. Z. Zhou, R. Rankin, and Y. F. Wang (2016), Interaction of ULF waves with different ion species: Pitch angle and phase space density implications, *J. Geophys. Res. Space Physics*, *121*, 9459–9472, doi:10.1002/2016JA022995.
- Roussos, E., et al. (2016), Quasi-periodic injections of relativistic electrons in Saturn's outer magnetosphere, *Icarus*, *263*, 101, doi:10.1016/j.icarus.2015.04.017.
- Russell, C. T., J. S. Leisner, C. S. Arridge, M. K. Dougherty, and X. Blanco-Cano (2006), Nature of magnetic fluctuations in Saturn's middle magnetosphere, *J. Geophys. Res.*, *111*, A12205, doi:10.1029/2006JA011921.
- Singer, H. J., C. T. Russell, M. G. Kivelson, E. W. Greenstadt, and J. V. Olson (1977), Evidence for the control of Pc3–4 magnetic pulsations by the solar wind velocity, *Geophys. Res. Lett.*, *4*, 377–379, doi:10.1029/GL0041009p00377.
- Sittler, E. C., Jr., et al. (2005), Preliminary results on Saturn's inner plasmasphere as observed by Cassini: Comparison with Voyager, *Geophys. Res. Lett.*, *32*, L14S07, doi:10.1029/2005GL022653.
- Sittler, E. C., Jr., et al. (2008), Ion and neutral sources and sinks within Saturn's inner magnetosphere: Cassini results, *Planet. Space Sci.*, *56*, 3.
- Southwood, D. J. (1974), Some features of field line resonances in the magnetosphere, *Planet. Space Sci.*, *22*, 483, doi:10.1016/0032-0633(74)90078-6.
- Southwood, D. J., and M. G. Kivelson (1981), Charged particle behavior in low frequency geomagnetic pulsations 1. Transverse waves, *J. Geophys. Res.*, *86*, 5643–5655, doi:10.1029/JA086iA07p05643.
- Southwood, D. J., and M. G. Kivelson (1982), Charged particle behavior in low frequency geomagnetic pulsations 2. Graphical approach, *J. Geophys. Res.*, *87*, 1707–1710, doi:10.1029/JA087iA03p01707.
- Southwood, D. J., and M. G. Kivelson (1990), The magnetohydrodynamic response of the magnetospheric cavity to changes in solar wind pressure, *J. Geophys. Res.*, *95*, 2301–2309, doi:10.1029/JA095iA03p02301.
- Southwood, D. J., and M. G. Kivelson (2007), Saturn magnetospheric dynamics: Elucidation of a camshaft model, *J. Geophys. Res.*, *112*, A12222, doi:10.1029/2007JA012254.
- Tamao, T. (1964), A hydromagnetic interpretation of geomagnetic SSC\*, *Rep. Ionos. Space Res. Jpn.*, *18*, 16–31.
- Thomsen, M. F., and J. A. Van Allen (1980), Motion of trapped electrons and protons in Saturn's inner magnetosphere, *J. Geophys. Res.*, *85*, 5831–5834, doi:10.1029/JA085iA11p05831.
- Thomsen, M. F., D. B. Reisenfeld, D. M. Delapp, R. L. Tokar, D. T. Young, F. J. Cray, E. C. Sittler, M. A. McGraw, and J. D. Williams (2010), Survey of ion plasma parameters in Saturn's magnetosphere, *J. Geophys. Res.*, *115*, A10220, doi:10.1029/2010JA015267.
- Thomsen, M. F., et al. (2014), Ion composition in interchange injection events in Saturn's magnetosphere, *J. Geophys. Res. Space Physics*, *119*, 9761–9772, doi:10.1002/2014JA020489.
- Thomsen, M. F., C. M. Jackman, D. G. Mitchell, G. Hospodarsky, W. S. Kurth, and K. C. Hansen (2015), Sustained lobe reconnection in Saturn's magnetotail, *J. Geophys. Res. Space Physics*, *120*, 10,257–10,274, doi:10.1002/2015JA021768.
- Tokar, R. L., et al. (2008), Cassini detection of water-group pick-up ions in the Enceladus torus, *Geophys. Res. Lett.*, *35*, L14202, doi:10.1029/2008GL034749.
- Villante, U., and M. Piersanti (2008), An analysis of sudden impulses at geosynchronous orbit, *J. Geophys. Res.*, *113*, A08213, doi:10.1029/2008JA013028.
- Waite, J. H., et al. (2006), Cassini ion and neutral mass spectrometer: Enceladus plume composition and structure, *Science*, *311*, 1419–1422, doi:10.1126/science.1121290.
- Wang, C., J. B. Liu, Z. H. Huang, and J. D. Richardson (2007), Response of the magnetic field in the geosynchronous orbit to solar wind dynamic pressure pulses, *J. Geophys. Res.*, *112*, A12210, doi:10.1029/2007JA012664.
- Wilson, R. J., R. L. Tokar, M. G. Henderson, T. W. Hill, M. F. Thomsen, and D. H. Pontius Jr. (2008), Cassini plasma spectrometer thermal ion measurements in Saturn's inner magnetosphere, *J. Geophys. Res.*, *113*, A12218, doi:10.1029/2008JA013486.
- Wilson, R. J., R. L. Tokar, and M. G. Henderson (2009), Thermal ion flow in Saturn's inner magnetosphere measured by the Cassini plasma spectrometer: A signature of the Enceladus torus?, *Geophys. Res. Lett.*, *36*, L23104, doi:10.1029/2009GL040225.
- Wilson, R. J., P. A. Delamere, F. Bagenal, and A. Masters (2012), Kelvin-Helmholtz instability at Saturn's magnetopause: Cassini ion data analysis, *J. Geophys. Res.*, *117*, A03212, doi:10.1029/2011JA016723.
- Yang, B., Q.-G. Zong, Y. F. Wang, S. Y. Fu, P. Song, H. S. Fu, A. Korth, T. Tian, and H. Reme (2010), Cluster observations of simultaneous resonant interactions of ULF waves with energetic electrons and thermal ion species in the inner magnetosphere, *J. Geophys. Res.*, *115*, A02214, doi:10.1029/2009JA014542.
- Yang, B., Q.-G. Zong, S. Y. Fu, X. Li, A. Korth, H. S. Fu, C. Yue, and H. Reme (2011a), The role of ULF waves interacting with oxygen ions at the outer ring current during storm times, *J. Geophys. Res.*, *116*, A01203, doi:10.1029/2010JA015683.
- Yang, B., et al. (2011b), Pitch angle evolutions of oxygen ions driven by storm time ULF poloidal standing waves, *J. Geophys. Res.*, *116*, A03207, doi:10.1029/2010JA016047.
- Yates, J. N., et al. (2016), Saturn's quasiperiodic magnetohydrodynamic waves, *Geophys. Res. Lett.*, *43*, 11,102–11,111, doi:10.1002/2016GL071069.
- Young, D. T., et al. (2004), Cassini plasma spectrometer investigation, *Space Sci. Rev.*, *114*, 1–112.
- Young, D. T., et al. (2005), Composition and dynamics of plasma in Saturn's magnetosphere, *Science*, *307*, 1262–1266, doi:10.1126/science.1106151.
- Zieger, B., and K. C. Hansen (2008), Statistical validation of a solar wind propagation model from 1 to 10 AU, *J. Geophys. Res.*, *113*, A08107, doi:10.1029/2008JA013046.
- Zong, Q.-G., Y. F. Wang, H. Zhang, S. Y. Fu, H. Zhang, C. R. Wang, C. J. Yuan, and I. Vogiatzis (2012), Fast acceleration of inner magnetospheric hydrogen and oxygen ions by shock induced ULF waves, *J. Geophys. Res.*, *117*, A11206, doi:10.1029/2012JA018024.